AGU
ADVANCING
EARTH AND
SPACE SCIENCES

JGR Atmospheres

Key Points:

- Over Maritime Continent land and sea, diurnal cycle amplitude typically peaks 2–3 days ahead of maximum MJO-induced daily mean precipitation
- Over Maritime Continent land, diurnal cycle amplitude typically peaks 3–6 days earlier than over surrounding seas
- Western (eastern) land areas experience their earliest diurnal precipitation maximum, whereas enhanced MJO convection is to the east (west)

Correspondence to:
A. J. Matthews,
a.j.matthews@uea.ac.uk

Modulation of the Observed Diurnal Cycle of Precipitation Over the Maritime Continent by the Madden-Julian Oscillation

Jack M. Mustafa[1,2] , Adrian J. Matthews[1,3] , Rob A. Hall[1] , Karen J. Heywood[1] , and Marina V. C. Azaneu[1,4]

[1]Centre for Ocean and Atmospheric Sciences, School of Environmental Sciences, University of East Anglia, Norwich, UK, [2]Institute for Climate and Atmospheric Science, School of Earth and Environment, University of Leeds, Leeds, UK, [3]School of Mathematics, University of East Anglia, Norwich, UK, [4]University of New South Wales, Sydney, NSW, Australia

Abstract The Madden-Julian oscillation (MJO) exerts a downscale influence on the diurnal cycle (DC) of precipitation over the Maritime Continent (MC). We assess the characteristics of this downscale influence in GPM-IMERG data across the western MC, comparing the MJO cycles of daily mean precipitation, DC amplitude, DC timing, and additional diurnal characteristics. During a typical MJO event, islands and surrounding waters experience their greatest DC amplitude 2–4 days ahead of their greatest daily mean precipitation. The MJO has a greater influence on daily mean precipitation over water and on DC amplitude over land. Greatest DC amplitude over land leads greatest DC amplitude over surrounding waters by 3–6 days. Diurnal cycle timing varies systematically by MJO phase in most locations, particularly eastern Sumatra, eastern Borneo and the eastern Makassar Strait where the diurnal maximum may systematically vary in timing by over 4 hours. Over these regions, the diurnal maximum propagates westward before, and eastward after, the active MJO crosses the western MC. As the active MJO crosses, the diurnal maximum gets earlier across western land on large islands, and later across eastern land, creating a west-east regime divide in DC timing variability. Additional diurnal characteristics quantify further changes in the nature of the diurnal oscillation. MJO-induced changes in the diurnal timing of convective cloud cover may influence local radiation budgets. These results provide a detailed benchmark for the modulation of the DC by the MJO against which this scale interaction in models may be assessed.

Plain Language Summary Tropical precipitation, particularly over the islands of Indonesia, is of great importance to global weather dynamics, and it is important to be able to predict tropical precipitation in weather models. Two sources of predictability for tropical precipitation are the diurnal cycle (DC) and the Madden-Julian oscillation (MJO). Good weather forecast models should be able to reproduce the DC and the MJO, as well as how the DC manifests at different stages of the MJO. In this study, satellite-derived precipitation is used to define the observed influence of the MJO on components of the DC. The strength of the DC is typically greatest slightly ahead of the strongest MJO precipitation. The timing of the diurnal precipitation maximum is also greatly influenced by the MJO, with the western sides of islands experiencing a late diurnal maximum and eastern sides of islands experiencing an early diurnal maximum in the early stages of the MJO, with this pattern reversing in the later stages of the MJO. Assuming that the DC of cloud cover exhibits a similar shift in DC timing, this shift will contribute to the influence of the MJO on local radiation budgets, with less land surface warming when diurnal activity peaks earlier in the afternoon.

1. Introduction

The archipelago of topographically complex islands straddling the Equator between Southeast Asia and Australia, known as the Maritime Continent (MC), experiences intense weather dynamics. In particular, during the boreal winter wet season, the islands and surrounding shallow seas of the MC receive more precipitation than any other region on Earth of comparable spatial extent. This poses a high risk of flooding and related natural disasters to local communities (Latos et al., 2021, 2023). Further, the intense weather dynamics over the MC drive global circulation patterns (Neale & Slingo, 2003; Ramage, 1968), and consequently, variability in MC weather dynamics leads to variable nature of the global circulation patterns that are induced. As such, there is substantial research interest in the modes of weather variability that exist over and around the MC.

One such mode of tropical weather variability is the Madden-Julian oscillation (MJO; Madden & Julian, 1971; Madden & Julian, 1972)—the dominant mode of intraseasonal weather variability between the Indian and Pacific oceans. The MJO consists of a broad region of enhanced convection and precipitation (often described as an "active envelope") that propagates eastward from the Indian Ocean, across the Maritime Continent into the western Pacific Ocean; this archetypal propagation is commonly segmented into eight MJO phases (P1–8) according to an MJO index such as the real-time multivariate MJO (RMM) index of Wheeler and Hendon (2004). Specific MJO phases have been statistically demonstrated to preferentially trigger (or, at least, precede) modes of variability elsewhere (e.g., Cassou, 2008; Neale & Slingo, 2003); for example, Skinner et al. (2022) evidence a strong link between P6 and the negative North Atlantic Oscillation (NAO−) weather mode, with a lag of order 10–15 days.

The MJO active envelope does not always complete its eastward propagation into the central-western Pacific; it frequently dissipates during P3–5 over the MC (e.g., Hendon & Salby, 1994; Hsu & Lee, 2005; Kim et al., 2014; Rui & Wang, 1990; Zhang & Ling, 2017). A number of mechanisms have been proposed to cause this blocking; these include physical blocking by topography (e.g., Kim et al., 2017; Wu & Hsu, 2009), reduced atmospheric moistening due to lower sea surface coverage (e.g., Birch et al., 2016; Sobel et al., 2010), a weakened zonal moisture gradient (e.g., Ahn et al., 2020; Gonzalez & Jiang, 2017; Kang et al., 2021), and interference of the strong MC diurnal cycle (DC).

A DC of atmospheric convection and precipitation is driven by warming of the land or sea surface by solar radiative forcing during daylight hours. Across the equatorial belt, diurnal surface warming is typically intense, especially over land. Around the MC, plentiful coastline results in a coastal diurnal regime (Kikuchi & Wang, 2008) where a strong sea breeze develops in the morning following sunrise, inducing convergence and ascent of moist air over land which destabilizes the atmospheric column and triggers deep convection and intense precipitation over land through the afternoon into the evening. A land breeze that develops in the evening then preferentially triggers convection and precipitation offshore overnight, often later into the night further from the coastline. Across the MC, it is therefore typically found that the composite DC of precipitation for a given location features one main maximum (during the afternoon/evening over land, and overnight over water) and one main minimum (Mustafa et al., 2024). As such, the DC is often summarized by its amplitude and the timing of the maximum (Love et al., 2011; Yang & Slingo, 2001). However, since convection and precipitation can initiate and terminate rapidly (Bai & Schumacher, 2022), it is found that the DC of precipitation features rapid transitions in many locations which are not well characterized by approximating the DC to a smooth first diurnal harmonic oscillation (Mustafa et al., 2024); for this reason, the "oscillatory nature" of the DC is also worth consideration.

By the DC mechanism described above, precipitation over land and near-coastal waters of the MC is "land-locked," meaning the driving dynamics are spatially fixed. There is therefore interference between propagating weather systems entering the MC, such as an MJO active envelope, and the land-locked DC dynamics, which frequently results in the weakening or total dissipation of the MJO active envelope. Even when the MJO active envelope is not blocked over the MC, its structure becomes much less coherent over the region.

Previous studies have demonstrated that the MJO exerts a downscale influence on the characteristics of the DC, particularly on its magnitude. Specifically, some studies have found that maximum DC amplitude within an MJO cycle tends to occur very slightly ahead of the point of maximum daily mean precipitation (Birch et al., 2016; Lu et al., 2019; Vincent & Lane, 2016); however, this phase lead is suggested not to be statistically significant across inland areas (Sakaeda et al., 2017). Some research indicates that the timing of the DC is also systematically influenced by the MJO (Oh et al., 2012; Rauniyar & Walsh, 2011; Sakaeda et al., 2017; Wei et al., 2020); however, other studies do not find a robust influence (Lu et al., 2019; Suzuki, 2009; Tian et al., 2006). A further body of research has demonstrated the sensitivity of MJO propagation to the magnitude of the DC (e.g., Hagos et al., 2016; Ling et al., 2019; Savarin & Chen, 2023). As such, the scale interaction between the DC and the MJO over the MC influences elements of global weather at the medium range. Any failure of weather models to accurately simulate this scale interaction risks degrading the quality of medium-range global weather forecasts.

In order to assess the accuracy of model simulations of the MJO-DC scale interaction, the observed nature of the scale interaction must be robustly quantified for reference. This study provides a detailed characterization of the downscale influence of the MJO on the DC of precipitation; changes in the amplitude, timing, and oscillatory nature (i.e., the manner in which the observed diurnal increase and decrease in precipitation differs from a first

harmonic oscillation) of the DC are quantified. In particular, by analyzing the interaction on a grid cell by grid cell basis, the results of this study provide clarity on the nature of the influence of the MJO on DC timing.

The structure of the remainder of this study is as follows: Section 2 describes the DC compositing methodology, introduces the components of the DC that are individually considered and details how the variability of these DC components across the MJO cycle can be quantified. Section 3 presents analysis of the MJO cycles of daily mean precipitation, DC amplitude, DC timing, and the oscillatory nature of the DC, and Section 4 discusses the holistic nature of DC variability observed across the MJO cycle and the likely physical processes leading to this variability.

2. Data and Methods

2.1. Data

Satellite-derived precipitation is sourced from the Integrated Multi-Satellite Retrievals for GPM (IMERG) v06 final run, with a 30-min temporal resolution and a 0.1° by 0.1° spatial resolution (Huffman et al., 2015; Tan et al., 2019). The RMM index (Wheeler & Hendon, 2004) is used to quantify the phase of the MJO; the OLR-based (outgoing longwave radiation) MJO index (OMI; Kiladis et al., 2014) was also considered and produced qualitatively comparable results in general, though some of the greatest contrasts are noted throughout Section 3. The RMM index and OMI were sourced from the Australian Bureau of Meteorology (www.bom.gov.au/climate/mjo) and the US National Oceanic and Atmospheric Administration (https://psl.noaa.gov/mjo/mjoindex) respectively. In order to consider the influence of each phase of the MJO on the DC, a composite DC of precipitation was calculated for each of the eight MJO phases using the days when the RMM index reports an amplitude of at least 1.0. Using IMERG data from each of the 19 DJF seasons between and including 2001–2002 and 2019–2020, each of the eight composite DCs incorporates at least 74 days (and up to 244 days) of data, which proves to be easily sufficient to isolate the influence of the MJO. The IMERG land-sea mask is used to define grid cells as either land or water; grid cells with at least 80% water surface coverage are considered water grid cells.

2.2. Cycle Characterization

Figure 1 illustratively introduces some of the main characteristics of the MJO cycle that are considered in this study. The three main diurnal characteristics that may be influenced by the MJO are daily mean precipitation (c; Figure 1a) and the amplitude and timing of the DC (A_{DC} and ϕ_{DC}; Figure 1b). Initially, each of these diurnal characteristics is considered to oscillate sinusoidally through an MJO cycle (i.e., following an "MJO harmonic"); hence, the variability of each of these diurnal characteristics is characterized with an amplitude (A_{MJO}) and a phase (ϕ_{MJO}) as annotated in Figure 1 (see Table 1 for a comprehensive guide to the symbols used in Figure 1 and throughout this study). ϕ_{MJO} marks the MJO phase of the maximum for daily mean precipitation and DC amplitude, and the MJO phase of the earliest DC timing. Crucially, ϕ_{MJO} need not be the same for any of the three main diurnal characteristics; in Figure 1, the earliest DC timing occurs in P1, leading maximum DC amplitude by one MJO phase which itself leads maximum daily mean precipitation by another MJO phase.

Assuming a typical MJO cycle duration (48 days) and a sinusoidally oscillating DC with no day-to-day variability other than that induced by the MJO, the reconstructed time-series of precipitation across a typical MJO cycle based on these sinusoidally oscillating diurnal characteristics would look like the idealized time-series in Figure 1a. The MJO cycle amplitudes and phases for daily mean precipitation, DC amplitude and DC timing are presented in Sections 3.1–3.3, respectively. In practice, the composite DC does not always demonstrate a close approximation to sinusoidal oscillation; following Mustafa et al. (2024), the "skew" ($-1 \leq \alpha_{DC} \leq 1$) and "spike" ($-1 \leq \beta_{DC} \leq 1$) asymmetry characteristics of the DC are considered in addition to the three main diurnal characteristics, and the variability of these asymmetry characteristics across the MJO cycle is presented in Section 3.4. In essence, positive DC skew indicates rapid intensification and more gradual weakening of precipitation, whereas positive DC spike indicates a brief but extreme precipitation maximum and a longer lasting precipitation minimum, and vice versa in the case of the negatives. Section 5 of Mustafa et al. (2024) provides a detailed explanation of the skew and spike characteristics.

Much like the DC, MJO cycles are not necessarily characterized well by a sinusoid, and representation and understanding of MJO cycles can be enhanced by considering their asymmetry characteristics. The skew of the MJO cycle ($-1 \leq \alpha_{MJO} \leq 1$) quantifies the relative duration of the spans of the MJO cycle when the diurnal
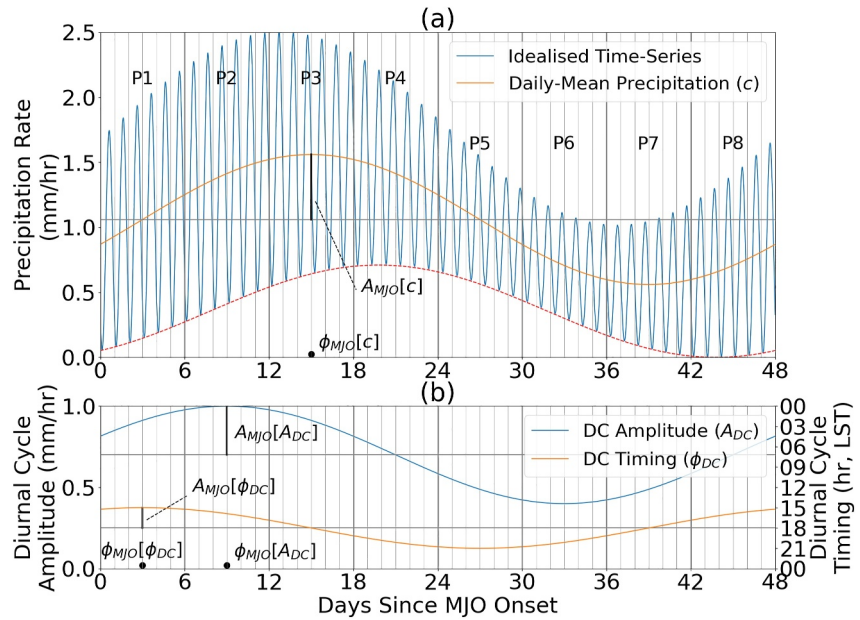
Figure 1. (a) Idealized time-series of precipitation (blue line) over a MC island through an idealized full MJO cycle (48 days; 6 days per MJO phase starting with P1). The orange line shows daily mean precipitation fed into the idealized time-series, which itself idealized to oscillate sinusoidally across the MJO cycle. $A_{MJO}(c)$ illustrates the amplitude of the MJO harmonic of daily mean precipitation (0.5 mm hr^{-1} in this example), and $\phi_{MJO}(c)$ marks the phase of the maximum of the same MJO harmonic (at day 15, corresponding to the middle of P3 which means 3.0 on the MJO phase scale). The red dashed line illustrates the non-diurnal contribution to precipitation. (b) The amplitude of the DC (blue) and the timing of its maximum (orange) used to force the idealized time-series in panel (a); each of these quantities is also idealized to oscillate sinusoidally across the MJO cycle, but not necessarily with the same MJO harmonic phase as each other or as daily mean precipitation (in this example, $\phi_{MJO}(A_{DC}) = 2.0$ and $\phi_{MJO}(\phi_{DC}) = 1.0$). The MJO harmonic amplitudes of DC amplitude ($A_{MJO}(A_{DC}) = 0.3$ mm hr^{-1}) and of DC timing ($A_{MJO}(\phi_{DC}) = 3$ hr) are also illustrated. Vertical gray lines mark midnight (local solar time, LST); every sixth vertical line is thicker to indicate an MJO phase transition. Horizontal lines indicate the mean of a DC parameter across the MJO cycle. A guide to the symbol nomenclature used in this figure and throughout the study is given in Table 1.

characteristic increases (or, for ϕ_{DC}, gets earlier) and decreases (or gets later). Positive α_{MJO} indicates rapid increase (or getting earlier) and gradual decrease (or getting later), and vice versa for negative α_{MJO}. The spike of the MJO cycle $\left(-1 \leq \beta_{MJO} \leq 1\right)$ quantifies the relative duration or extremity of the MJO cycle peak and trough. Positive β_{MJO} indicates a brief and intense maximum (or shift to an earlier diurnal timing), and vice versa for negative β_{MJO}. The skew- and spike-permitting waveforms are only considered when they differ substantially from the MJO harmonic (i.e., when $|\alpha_{MJO}| > 0.3$ or $|\beta_{MJO}| > 0.3$). Further, since these single-peak waveforms may not be appropriate for MJO cycles with multiple major peaks per MJO cycle, a measure of the MJO cycle variance explained by the waveform is calculated and only waveforms meeting a given threshold are considered, following Mustafa et al. (2024).

As a result of the range of cycle characterizations considered, multiple definitions exist for both amplitude and phase of the MJO cycle, and amplitude and timing of the DC. Three of these definitions are associated with a waveform approximation, and the fourth is referred to as a "basic characteristics" characterization and is based on the cycle maximum and minimum. For instance, the phase of an MJO cycle could be quantified using the basic characteristic—the MJO phase with the maximum/earliest DC parameter value ($\phi_{MJO,bc}$, an integer in the range 1–8)—the phase of the first MJO harmonic $\left(0.5 \leq \phi_{MJO,fh} < 8.5\right)$, or the phase of either the best-fitting skew-permitting or best-fitting spike-permitting waveform ($0.5 \leq \phi_{MJO,sk} < 8.5$ or $0.5 \leq \phi_{MJO,sp} < 8.5$). For the DC, the basic characteristics—termed "half range" and "peak time" following Mustafa et al. (2024)—are considered the default, but results have been considered for all measures of DC amplitude and timing, with key contrasts discussed. For the MJO cycle, the MJO harmonic amplitude and phase of the MJO harmonic are treated as the default amplitude and phase definitions and form the basis of most results presented, but like for the DC, the other measures of amplitude and phase are considered throughout and remarked on where noteworthy.

Table 1
A Guide to the Use of Symbolic Expressions in This Study

Expression	Meaning
MJO cycle descriptors	
A_{MJO}	Amplitude of the MJO cycle (of an unspecified DC parameter), quantified by $A_{MJO,fh}$ by default
$A_{MJO,fh}$	Amplitude of the first harmonic of the MJO cycle (of an unspecified DC parameter)
$A_{MJO,bc}$	Half the difference between the maximum and minimum (of an unspecified DC parameter) across the eight MJO phases
$A_{MJO,sk}$	Amplitude of the best-fitting skew-permitting waveform of the MJO cycle (of an unspecified DC parameter)
$A_{MJO,sp}$	Amplitude of the best-fitting spike-permitting waveform of the MJO cycle (of an unspecified DC parameter)
ϕ_{MJO}	Phase of the MJO cycle (of an unspecified DC parameter), quantified by $\phi_{MJO,fh}$ by default
$\phi_{MJO,fh}$	MJO phase when the first harmonic of the MJO cycle (of an unspecified DC parameter) peaks
$\phi_{MJO,bc}$	MJO phase of maximum[a] (of an unspecified DC parameter)
$\phi_{MJO,sk}$	MJO phase when the best-fitting skew-permitting waveform of the MJO cycle (of an unspecified DC parameter) peaks
$\phi_{MJO,sp}$	MJO phase when the best-fitting spike-permitting waveform of the MJO cycle (of an unspecified DC parameter) peaks
α_{MJO}	Skew parameter describing the asymmetry in duration of increase and decrease (of an unspecified DC parameter) through the MJO cycle
β_{MJO}	Spike parameter describing the asymmetry in duration of the high and low values (of an unspecified DC parameter)
DC parameters	
c	Daily mean precipitation
A_{DC}	"DC amplitude", quantified by $A_{DC,bc}$ by default
$A_{DC,bc}$	Diurnal "half range": half the difference between the diurnal maximum and minimum
$A_{DC,fh}$	Amplitude of the first diurnal harmonic
$A_{DC,sk}$	Amplitude of the best-fitting skew-permitting waveform of the DC
$A_{DC,sp}$	Amplitude of the best-fitting spike-permitting waveform of the DC
ϕ_{DC}	"DC timing", quantified by $\phi_{DC,bc}$ by default
$\phi_{DC,bc}$	Diurnal "peak time": time of day with maximum precipitation
$\phi_{DC,fh}$	Time of day when the first diurnal harmonic peaks
$\phi_{DC,sk}$	Time of day when the best-fitting skew-permitting waveform of the DC peaks
$\phi_{DC,sp}$	Time of day when the best-fitting spike-permitting waveform of the DC peaks
α_{DC}	Skew parameter describing the asymmetry in duration of diurnal precipitation rate increase and decrease
β_{DC}	Spike parameter describing the asymmetry in duration of the high precipitation and low precipitation
Examples of combined expressions	
$A_{MJO,fh}(c)$	Amplitude of the first harmonic of the MJO cycle of daily mean precipitation
$\phi_{MJO,sk}(A_{DC,bc})$	MJO phase when the best-fitting skew-permitting waveform of the MJO cycle of diurnal half-range peaks

Note. The uppermost group of expressions quantify features of the variability of a given DC parameter through the MJO cycle. The central group of expressions quantify features of the DC (which may vary between MJO phases). The lowermost group of expressions combine an MJO cycle descriptor from the uppermost group with a DC parameter from the central group; many combinations are possible, so a pair of examples are given. [a]Or, when the DC parameter is among the ϕ_{DC} group, MJO phase of earliest DC timing.

2.3. Approaches to Averaging

For calculations of an MJO cycle averaged over a given area, the mean of the DC parameter of interest is calculated for each MJO phase, instead of calculating the spatial-mean DC across the area and then computing the DC parameter of interest of that (i.e., mean of a parameter, not parameter of a mean). This approach allows for the spread of DC parameter values across the area in each MJO phase to be represented. For a given area of interest (e.g., Sumatra or the Java Sea), a polygon was constructed around the region, and grid cells within the polygon and on the appropriate side of the 80% water surface coverage threshold (see Section 2.1) were considered, with each grid cell equally weighted. Polygons for water regions are shown in Figure 2b, and polygons for island regions are not shown but tightly constrain each island to avoid incorporating small nearby islands.

Quantifying the average of cyclic variables, such as DC timing, DC timing difference, MJO phase, and MJO phase difference with a linear mean is not reliable. For such cyclic variables, a "polar mean" is calculated—as if each value to be averaged were located at equal radius on a circle, the "center of mass" calculated, and the radial angle of the center of mass taken to correspond to the polar mean.

In order to properly account for cyclicity in the calculation of the MJO harmonic of DC timing and to avoid complications arising from the DC timing varying either side of local midnight at some locations, the polar mean of each set of eight DC timing values was determined and each individual DC timing value was shifted by 24 hr if necessary to fall within 12 hr of the polar mean. For instance, if the polar mean of the eight DC timing values at a location was 22.0 but the DC timing was 1.0 during one MJO phase, 1.0 would be replaced with 25.0 to calculate the MJO harmonic.

Calculations are performed in coordinated universal time (UTC) and later converted to local solar time (LST) as a linear function of longitude (or mean longitude for calculations across several grid cells).

3. Results

3.1. Influence of the MJO on Daily Mean Precipitation

Across the western MC region, 68% of land area experiences maximum daily mean precipitation during either P2 or P3, whereas 71% of marine area experiences maximum precipitation during either P3 or P4, and the MJO harmonic phase is typically close to this maximum (Figure 2). The MJO cycle of daily mean precipitation over land precedes that over water by nearly one MJO phase ($\phi_{MJO,fh}(c) = 2.6$ over land, and $\phi_{MJO,fh}(c) = 3.4$ over water), or about one tenth of an MJO cycle. There is notable disagreement in the MJO harmonic phase of daily mean precipitation over water between the RMM index and OMI; whereas, similar over the Indian Ocean, the OMI reports an MJO phase often over half an MJO phase later across the Java Sea and often over a whole MJO phase later across the South China Sea (not shown). As such the MJO harmonic phase lag relative to land slightly exceeds one MJO phase when the OMI is used in place of the RMM index to define MJO phase, with the spatial-mean MJO harmonic phase over land scarcely affected, whereas that over water is pushed back from 3.4 to 3.8.

Daily mean precipitation is typically larger over land than water across the western MC region, especially during suppressed MJO conditions in P8–1; this is attributed to strong diurnal forcing under comparatively clear skies, which induce strong sea breezes that result in moisture convergence over land. However, the amplitude of the MJO cycle of daily mean precipitation is nearly 50% stronger over water than over land ($A_{MJO,fh}(c) = 0.12$ mm h^{-1} over land, and $A_{MJO,fh}(c) = 0.17$ mm h^{-1} over water; white lines in Figures 2c and 2d). This leads to drier conditions over land than water during P4, whereas the MJO active envelope is over the western MC, on average; cloudier skies within the active envelope inhibit the diurnal forcing mechanism, resulting in weaker moisture convergence over land.

There is substantial variability in the MJO cycle of daily mean precipitation between different bodies of land and water (Figure 2). Although the amplitude and phase of the MJO cycle of daily mean precipitation are reasonably uniform across both Sumatra and Java, there is a clear regime divide between western and eastern Borneo, either side of approximately 115°E, with the MJO cycle over western Borneo being stronger and earlier in MJO phase. This regime divide is most defined north of the Equator, where it loosely follows the eastern side of northern-to-central Borneo's broad region of high topography. Averaging across western Borneo (west of 115°E), precipitation tends to be stronger during P1–4 than during P5–8 at all times of day (Figure 3c) producing a
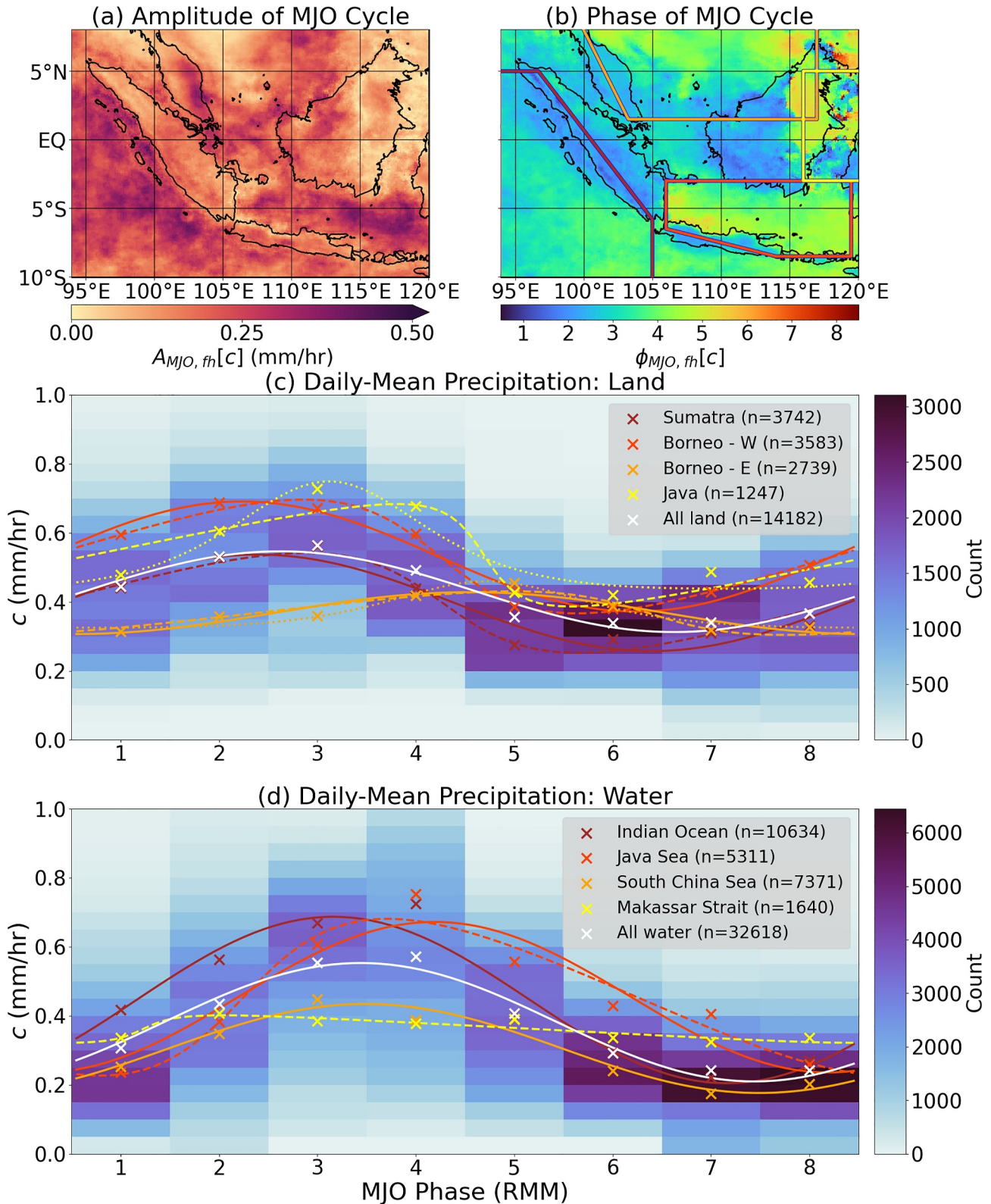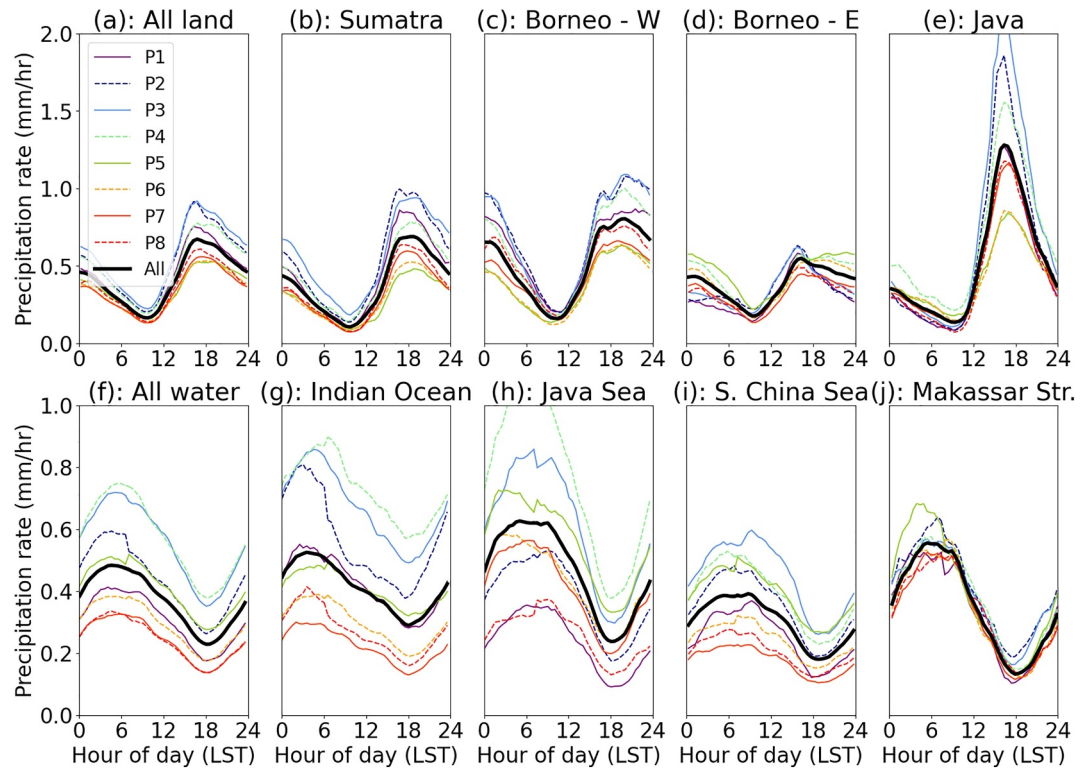
Figure 2.

Figure 3. Spatial-mean composite DC of precipitation for each MJO phase for each of five land regions (top row) and five water regions (bottom row) within the western MC. Borneo is divided either side of 115°E, and water regions are outlined in Figure 2b, with an 80% water surface coverage threshold used to distinguish land and water cells. Each black line shows the spatial-mean climatological DC for DJF, including inactive MJO days. Each spatial mean is calculated in UTC, and converted to LST according to the mean longitude of the region considered. Note the different vertical axis scales for the top and bottom row.

high-amplitude MJO cycle of daily mean precipitation (see the red line in Figure 2c). Over eastern Borneo (Figure 3d), the hours around midday while diurnal precipitation is intensifying are also wettest during P1–3; however, overnight hours are wettest during P4–6, averaging out to produce a low-amplitude MJO cycle of daily mean precipitation ($A_{MJO,fh}(c) = 0.06$ mm h^{-1}; the orange line in Figure 2c) compared with western Borneo, Sumatra, and Java ($A_{MJO,fh}(c)$ between 0.13 and 0.17 mm h^{-1}). Zhou et al. (2023) also demonstrate this regime divide in precipitation over Borneo; they note that the transition from more precipitation across the west up to P4 to more precipitation across the east from P5 aligns with a reversal in the low-level wind direction over the island from easterly to westerly. Topography-free simulations in their study show that the regime divide would not occur over a flattened island; therefore, there is high confidence that this regime divide results from the downwind orographic enhancement of precipitation (Ichikawa & Yasunari, 2006). However, the absence of an analogous eastern regime to the east of Sumatra's Barisan mountain range suggests that additional factors are responsible.

Sumatra, western Borneo, eastern Borneo and Java each, on average, experience a rapid weakening of daily mean precipitation following their local maximum, meaning that the MJO cycle may be described well using the skew-permitting waveform with negative skew parameter (dashed lines in Figure 2c). For Java, where a rapid drop-off

Figure 2. Variability of daily mean precipitation rate by MJO phase. Top row: the (a) amplitude and (b) phase of the MJO harmonic of daily mean precipitation. The brown, red, orange and yellow polygons in (b) outline the regions containing the waters defined as the Indian Ocean, the Java Sea, the South China Sea, and the Makassar Strait, respectively. Borneo is divided either side of 115°E. See Section 2.3 for further details on region definitions (c) and (d) Histograms of daily mean precipitation rate across the eight MJO phases over land and water, respectively. "Count" denotes the number of grid cells in a histogram bin, and n denotes the number of grid cells counted toward a region. Crosses show the spatial-mean daily mean precipitation by region for each MJO phase. Solid lines follow the MJO harmonic for each region, whereas dashed and dotted lines follow the best-fitting skew-permitting and best-fitting spike-permitting waveforms for each regional MJO cycle, respectively. Only waveforms that sufficiently accurately characterize the MJO cycle variability are shown ($\epsilon \leq 0.4$; Equation 2 of Mustafa et al. (2024)). Asymmetric waveforms are only presented if the magnitude of the asymmetry parameter exceeds 0.3.

in precipitation is observed between P3 and P5 (Figure 3e), the strength of this asymmetry ($\alpha_{MJO}(c) = -0.61$) results in the MJO phase of maximum daily mean precipitation being almost one MJO phase later based on the best-fitting skew-permitting waveform (dashed yellow line in Figure 2c, $\phi_{MJO,sk}(c) = 3.8$) than based on either the best-fitting spike-permitting waveform (dotted yellow line, $\phi_{MJO,sp}(c) = 3.1$) or the MJO harmonic (not shown due to poor characterization, $\phi_{MJO,fh}(c) = 2.9$). $\alpha_{MJO}(c)$ falls between -0.36 and -0.34 for the other averaged land regions. The MJO phase of the best-fitting skew-permitting waveform spans from 2.9 over both Sumatra and western Borneo, through 3.8 over Java, to 5.0 over eastern Borneo. Although the MJO phases of maximum daily mean precipitation either side of Borneo are only a quarter of an MJO cycle apart, the rapid weakening means that minimum daily mean precipitation over western Borneo occurs very shortly after maximum daily mean precipitation over eastern Borneo.

Over water, P4 is the dominant phase for maximum daily mean precipitation south of 2°S across the western MC region's span of longitudes (Figure 2b). Within a few degrees of the Equator and especially immediately west of the large islands, maximum daily mean precipitation generally occurs slightly earlier in the MJO cycle than over surrounding waters. There is more regional variability further north, with maxima mostly between P2 and P5. The major water bodies within the western MC region—the Indian Ocean, the South China Sea, the Java Sea, and the Makassar Strait (outlined in Figure 2a)—show composite MJO harmonic phases ($\phi_{MJO,fh}(c)$) of 3.2, 3.5, 4.2 and 3.3, respectively. Unlike for the land regions, no strong systematic asymmetry in the MJO cycle of daily mean precipitation is found for any of these water bodies (i.e., $|\alpha_{MJO}(c)| < 0.3$), with the exception of the Makassar Strait where the amplitude of the MJO cycle is very low.

3.2. Influence of the MJO on the Amplitude of the Diurnal Cycle

The MJO harmonic phase of the spatial-mean DC amplitude ($\phi_{MJO,fh}(A_{DC,bc})$) over land is 2.2 (Figure 4c), and over water the equivalent phase is 2.8 (Figure 4d). These MJO harmonic phases are slightly earlier than the corresponding phases for the cycle of daily mean precipitation (i.e., $\phi_{MJO,fh}(A_{DC,bc}) < \phi_{MJO,fh}(c)$), implying that DC amplitude has peaked and begun to decrease before daily mean precipitation reaches its maximum. The MJO harmonic of DC amplitude precedes the MJO harmonic of daily mean precipitation in most locations at the IMERG grid-cell resolution; over 74% of western MC land area and 85% of marine area (Figure 5b). The mean MJO phase lag of daily mean precipitation behind DC amplitude over both land and water averages around half an MJO phase, with mean lags of 0.44 and 0.50 MJO phases, respectively. There is more regional variability over land than over water; parts of eastern Borneo experience the most extreme MJO phase lags observed across the region, whereas western Borneo generally shows an MJO phase lag close to zero. Both Sumatra and Java show a small but consistent MJO phase lag close to their coastlines, tending toward being in phase or slight phase lead of the MJO cycle of daily mean precipitation further inland. The magnitude of these MJO phase lags is lessened slightly (to as low as 0.23 over land and 0.40 over water) when the DC amplitude is quantified with any waveform amplitude instead of the diurnal half range. The MJO phase lag observed in most locations is consistent with previous studies (e.g., Birch et al., 2016; Vincent & Lane, 2017), as is the lack of clear phase lag across western Borneo and inland locations (Sakaeda et al., 2017). The phase lag has been attributed to a weakening of diurnal forcing (and therefore DC amplitude) when the leading edge of the MJO active envelope arrives, whereas conditions for (large-scale or non-diurnal) precipitation continue to become more favorable between the arrival of the leading edge of the envelope and its center. Across western Borneo and other inland locations without such a phase lag, the DC amplitude tends to vary at least as much as daily mean precipitation through the MJO cycle (Figure 6b), meaning that the non-diurnal component of precipitation (i.e., the red dashed line in an observed version of Figure 1a) does not increase within the active envelope. This implies that the contribution of the MJO to increased precipitation across these locations is entirely due to increased diurnal activity and that the large-scale conditions are less directly impactful in these locations than elsewhere.

Like for daily mean precipitation, defining MJO phase with the OMI yields a substantially later spatial-mean MJO harmonic phase of DC amplitude over water (3.5 instead of 2.8), such that the phase lag measured between the MJO harmonics of DC amplitude and daily mean precipitation is similar as for the RMM index. This difference is likely the result of a slight longitudinal offset between the OLR components of the empirical orthogonal functions (EOFs) associated with MJO P3 (negative EOF2 of the RMM index and negative EOF1 of the OMI); P3 commences with the OLR minimum (marking the center of the MJO active envelope) further west according to the average OMI EOF1 than the RMM EOF2 (Stachnik & Chrisler, 2020). This can explain why the phases do not
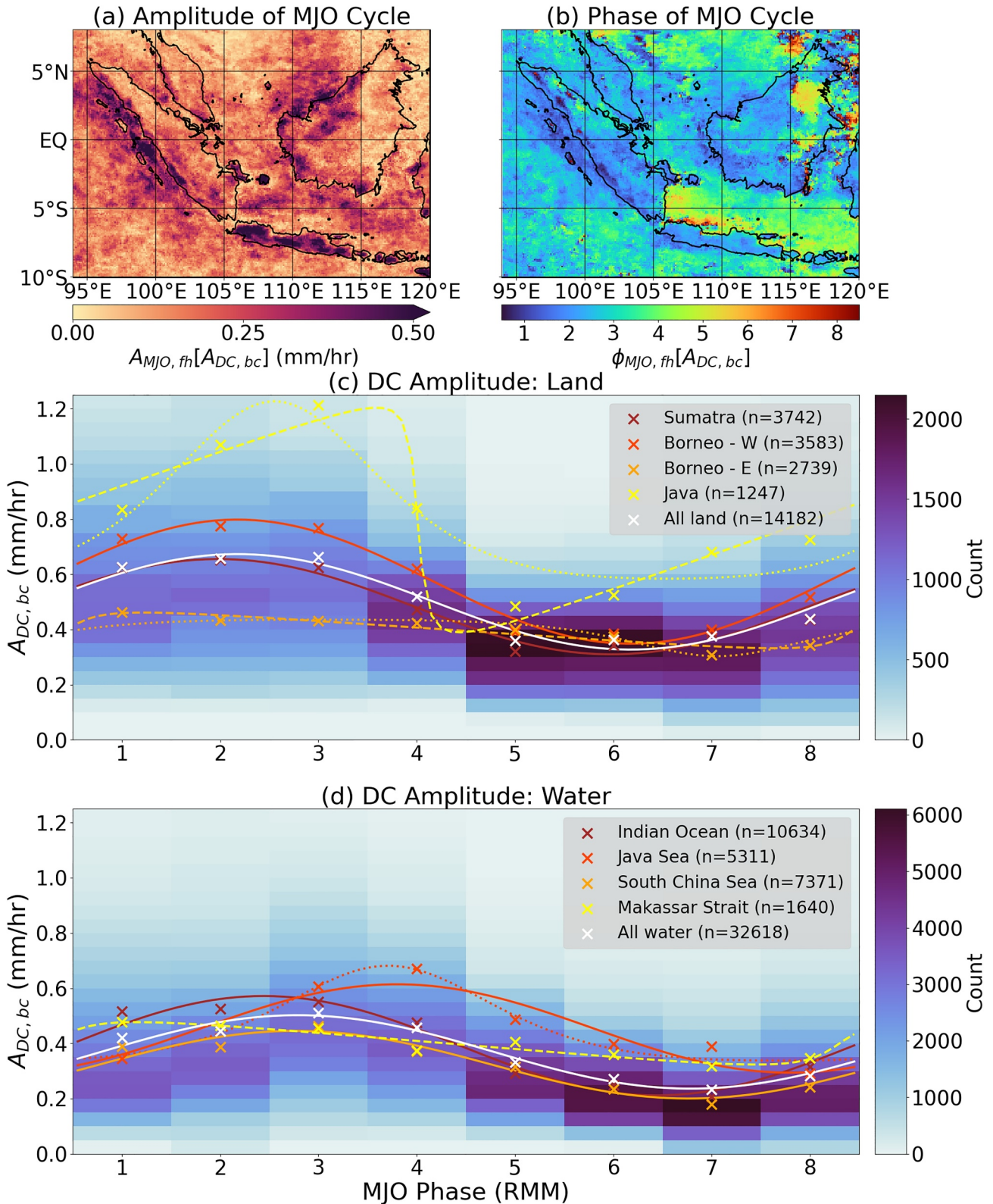
Figure 4. As for Figure 2, but for the variability of DC amplitude (as measured by the half range; $A_{DC,bc}$ in Table 1) by MJO phase.
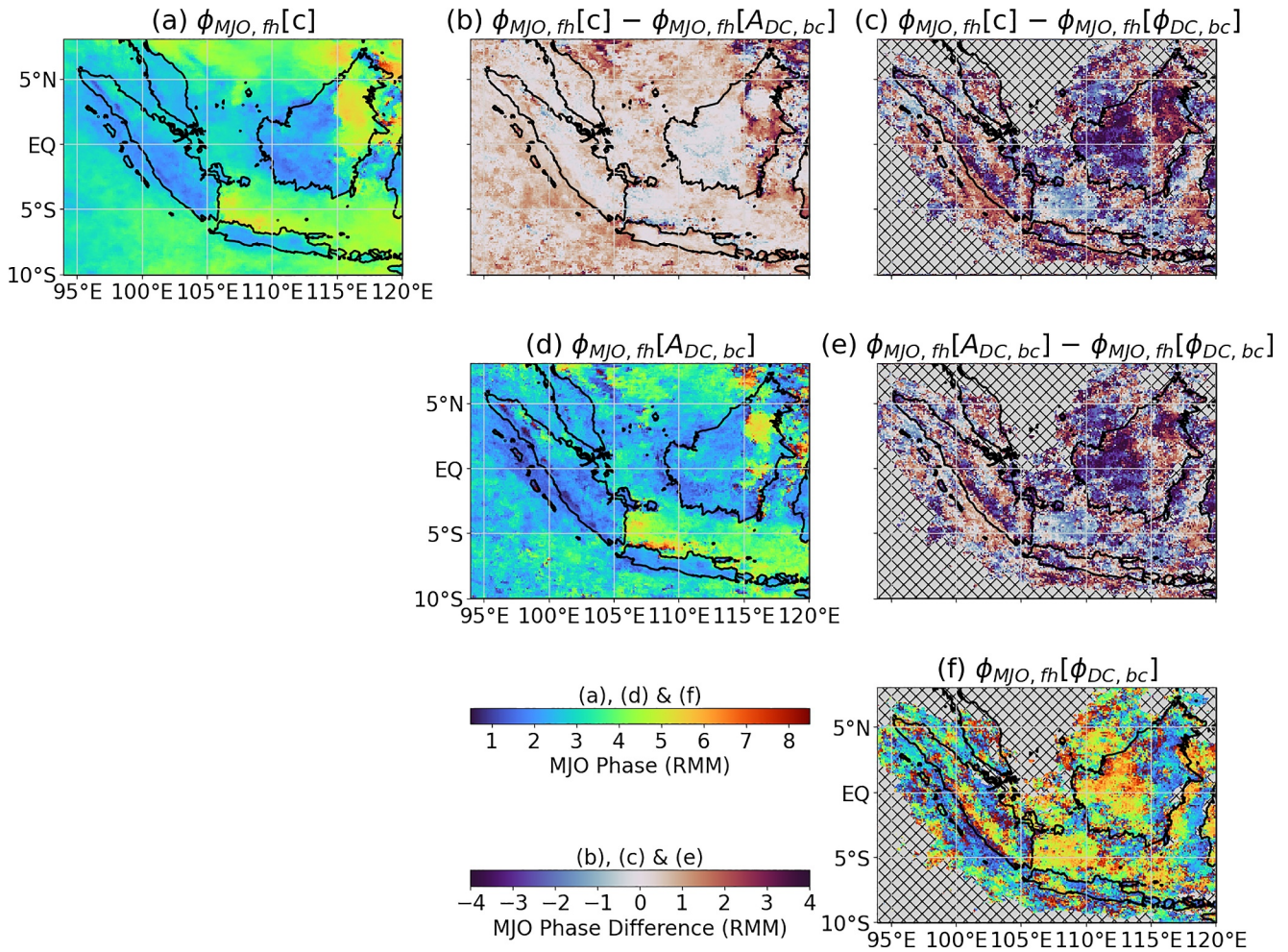
Figure 5. Comparison of the phase of the MJO cycles of daily mean precipitation, DC amplitude and DC timing. The leftmost panel in each row shows the MJO harmonic phase of the MJO cycle of (a) daily mean precipitation (c), (d) the DC half range ($A_{DC,bc}$), and (f) the DC peak time ($\phi_{DC,bc}$). Remaining panels (b, c, e) compare the MJO harmonic phases and show their phase lags. Locations with weak diurnal activity ($A_{DC,bc} < 0.15$ mm h^{-1}) are hatched over in the right column since the diurnal maximum is typically less pronounced and DC timing is therefore more susceptible to noise.

precisely align between the two MJO indices, but not why the MJO index dependence appears stronger over water than over land. It is likely that the inclusion of dynamical variable fields (u_{850} and u_{200}) in the RMM index but not in OMI is the cause; the maximum in DC amplitude is known to lead the OLR minimum over land but not water (Peatman et al., 2014); however, land and water have not been shown to have similarly contrasting phase lag relationships for the dynamical components of the RMM EOFs, therefore the inclusion of these dynamical components may dilute the land-sea contrast in the MJO harmonic phase.

The amplitude of the MJO harmonic of DC amplitude shows substantial regional variability (Figure 4a). The strongest MJO cycles of DC amplitude are over Java (Figure 3e), Indian Ocean waters close to the west Sumatra coast, parts of onshore and offshore northwest Borneo, some of the smaller islands, and the northern stretch of the Java Sea (Figure 3h). Weaker MJO cycles in DC amplitude are found over eastern Borneo (Figure 3d), parts of north and east Sumatra, the southern stretch of the Java Sea, and the west South China Sea (Figure 3i). Some of these areas of high and low variability of DC amplitude align with areas of high and low variability of daily mean precipitation (Figure 2a); however, some areas, such as Java, experience a strong MJO cycle of DC amplitude in spite of a moderate MJO cycle of daily mean precipitation, quantified by a high ratio between the MJO harmonic amplitudes of DC amplitude and daily mean precipitation (Figure 6b). In general, land areas, especially over Java, high topography and small islands, experience a stronger MJO cycle in DC amplitude, whereas marine locations typically experience a stronger MJO cycle in daily mean precipitation, especially far offshore. The MJO harmonic
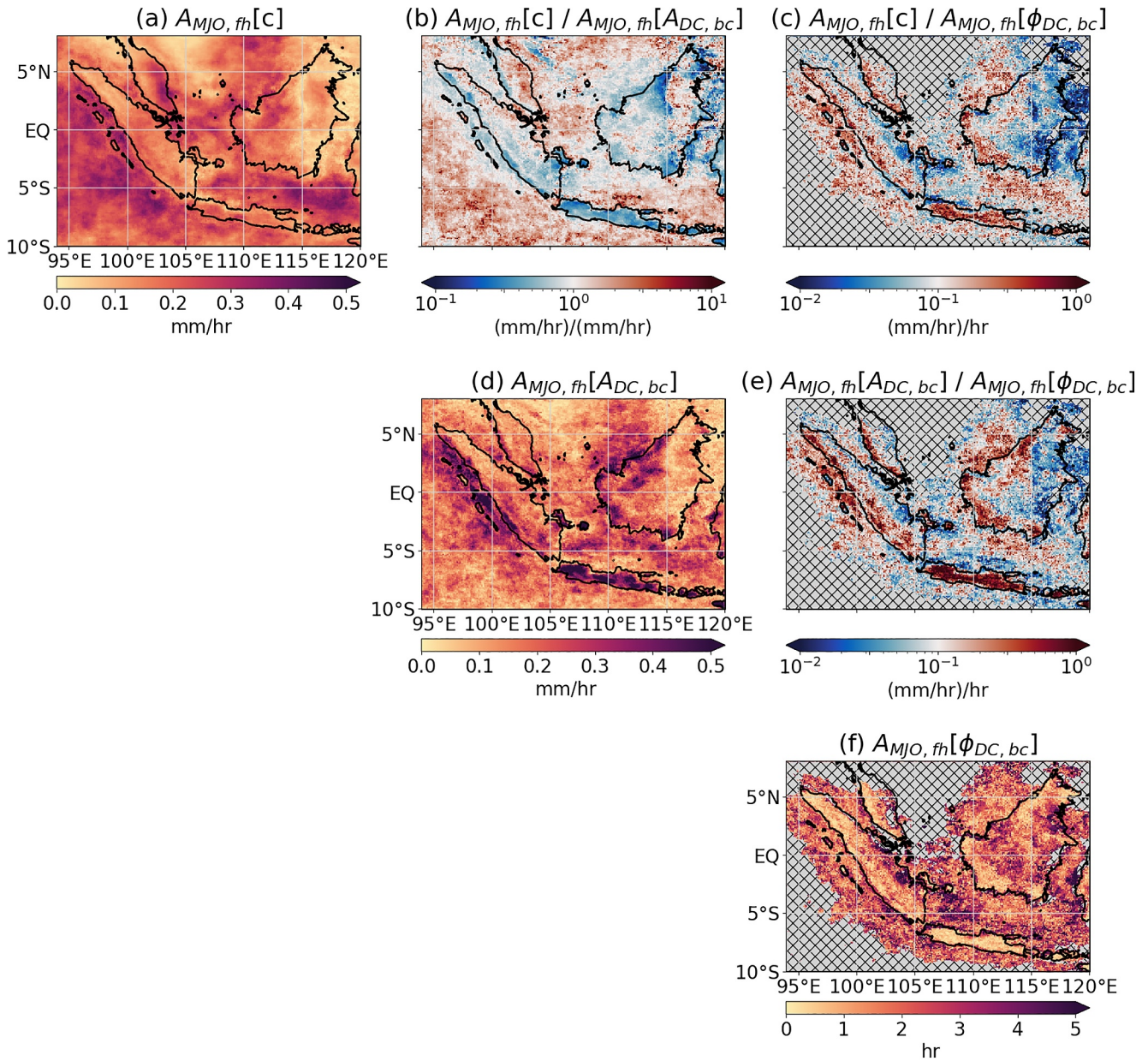
Figure 6. As for Figure 5, but for (a,d,f) MJO harmonic amplitudes, and (b, c, e) MJO harmonic amplitude ratios. Like in Figure 5, the right column is hatched where diurnal activity is weak.

amplitude of the spatial-mean DC amplitude ($A_{MJO,fh}(A_{DC,bc})$) over land is 0.17 mm h^{-1} (Figure 4c); however, the individual land regions have spatial-mean MJO harmonic amplitudes ranging from 0.06 mm h^{-1} (eastern Borneo) to 0.30 (Java). Over water, the amplitude of the MJO harmonic of spatial-mean DC amplitude is 0.13 mm h^{-1} (Figure 4d), with the Indian Ocean and Java Sea areas both showing slightly above-average MJO harmonic amplitude. Although subtle, the difference between the MJO harmonic amplitude over land and water across the western MC region is found to be statistically significant at the 95% confidence level ($p = 0.025$), accounting for auto-correlation of nearby grid cells by downsampling according to a characteristic correlation length scale of 1°; however, significance calculations over smaller regions show variable results. Java experiences a substantially greater MJO harmonic amplitude of DC amplitude than its surrounding waters (a highly significant difference), whereas Borneo and its surrounding waters experience a similar amplitude (low/no significant difference), and Sumatra has a weaker amplitude than the waters immediately to its west (a significant difference of the opposite

nature). The remarkably high MJO harmonic amplitude of DC amplitude over waters west of Sumatra is due to the offshore propagation of precipitation, which is very strong and frequent around P8–2 but negligible around P5–6; in contrast, the DC over Sumatran land does not show the same extreme amplitude variability (Peatman et al., 2021).

There is a similar tendency toward negative skew of the MJO cycle of DC amplitude over land as was noted for the MJO cycle of daily mean precipitation over land. In particular, Java shows a rapid weakening of diurnal variability between P3 and P5 ($\alpha_{MJO}(A_{DC,bc}) = -0.84$; however, the precise extremity of this asymmetry cannot be accurately quantified without resolving changes to DC amplitude through the MJO cycle in more than 8 phases); this is similar to the rapid weakening of daily mean precipitation over Java between P3 and P5 ($\alpha_{MJO}(A_{DC,bc}) = -0.61$). The Java Sea shows an especially high DC amplitude in P4 (Figure 4d), which correlates with the high daily mean precipitation it also experiences in this MJO phase (Figure 2d).

3.3. Influence of the MJO on the Timing of the Diurnal Cycle

One complicating factor affecting these results is that the DC timing is highly susceptible to noise where the DC is weak. For example, offshore areas, which are known to experience weak diurnal variability, often produce high MJO harmonic amplitudes for DC timing. Results here only consider locations where the DC amplitude (in the DJF climatological composite) exceeds a threshold of 0.15 mm h^{-1}. Nevertheless, it is not straightforward to identify areas that experience a systematic MJO influence on DC timing based on the MJO harmonic amplitude alone (Figure 7a). Spatial coherence of the MJO harmonic phase (Figure 7b) helps to distinguish such areas. Although the MJO harmonic phase of DC timing is less spatially coherent than that of either daily mean precipitation or DC amplitude (Figure 5), areas of coherence exist across the west Java Sea (P4–6), western and eastern Borneo (P5–6 and P2–3, respectively), the Makassar Strait (P5–6 and P2–3 along the west and east sides, respectively), western and eastern Sumatra (P4–7 and P1–2), and Indian Ocean waters close to the southwest coast of Sumatra (P1–2). Most of these locations have a consistently high MJO harmonic amplitude across the region (Figure 7a). In contrast, many near-coastal land areas across the west side of the large islands have a small MJO harmonic amplitude.

Since different areas of land and of water exhibit MJO cycles of DC timing with such different phasing, it is unsurprising that much of this variability cancels out in the spatial-mean MJO cycles over land and water, such that DC timing appears only subtly dependent on the MJO phase. Over land, the MJO cycle of DC timing is well characterized by the best-fitting skew-permitting waveform, which has an amplitude ($A_{MJO,sk}(\phi_{DC,bc})$) of 0.59 hr, a phase ($\phi_{MJO,sk}(\phi_{DC,bc})$) of 2.0 and a skew ($\alpha_{MJO}(\phi_{DC,bc})$) of −0.33 (white dashed line in Figure 7c). This characterizes a change of slightly over 1 hour in the timing of maximum diurnal precipitation over land across the MJO cycle, with an earliest spatial-mean DC timing of 17.7 hr in P2 and latest spatial-mean DC timing of 19.2 hr in P5. Both Sumatra and Java experience an MJO cycle in spatial-mean DC timing with similar characteristics to the spatial-mean land cycle, albeit over 1 hour earlier in the day in the case of Java. The DC composited over Java for each MJO phase (Figure 3e) demonstrates consistent timing of the diurnal maximum in the late afternoon, but a subtle coherent shift in DC timing is nonetheless noted. The MJO cycle of spatial-mean DC timing over eastern Borneo has a similar phase ($\phi_{MJO,sk}(\phi_{DC,bc}) = 2.4$) and a similar negative skew ($\alpha_{MJO}(\phi_{DC,bc}) = -0.43$), inferring rapid progression of DC timing to later in the evening following P2. The timing of the spatial-mean diurnal maximum over eastern Borneo (Figure 3d) varies more visibly by MJO phase than over Java. During P1–3, an afternoon maximum is followed by rapid weakening of precipitation through the evening, whereas during P4–6, the period of high precipitation is prolonged through the night. The MJO cycle of spatial-mean DC timing over eastern Borneo (orange dashed line in Figure 7c) shows a much more pronounced amplitude ($A_{MJO,sk}(\phi_{DC,bc}) = 2.1$ hr), oscillating between a spatial-mean DC timing of 16.4 hr in P2 and 20.7 hr in P5. The MJO cycle of spatial-mean DC timing over western Borneo is out of phase with the other land regions considered; the earliest spatial-mean DC timing (19.4 hr) occurs in P5, whereas the latest spatial-mean DC timing (21.1 hr) occurs in P1. If, like for Sumatra and Java, the spatial-mean DC timing across all of Borneo is considered in each MJO phase, the strong but opposing variability in each of the two regimes approximately cancels out to produce a weak spatial-mean MJO cycle in DC timing, slightly favoring the eastern regime. Sumatra clearly shows the same west-east regime divide as Borneo, and to a lesser extent, there is evidence of longitudinal influence on MJO harmonic phase of DC timing over Java (Figure 7b).
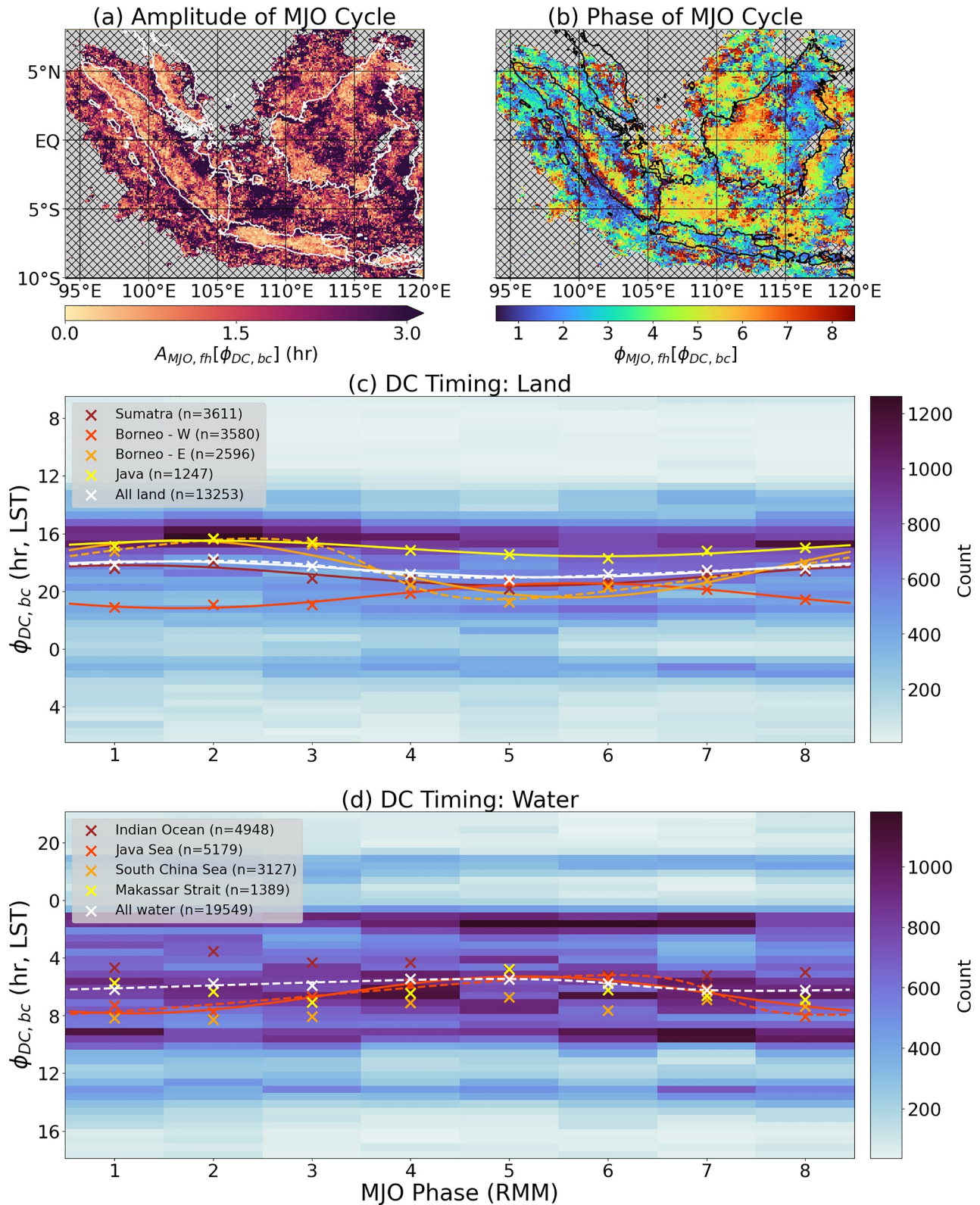
Figure 7. As for Figure 2, but for the variability of DC timing (as measured by the peak time; $\phi_{DC,bc}$ in Table 1) by MJO phase. Locations with weak diurnal activity ($A_{DC,bc} < 0.15$ mm h^{-1}) are hatched over in panels (a and b). For each MJO phase, crosses show the spatial mean of the DC timing distribution for locations with sufficiently strong diurnal activity, and the vertical axis is set to center on the polar mean of the eight all-encompassing MJO phase spatial means (white crosses). Time progresses downwards in panels (c and d).

The MJO cycle of spatial-mean DC timing over water is very subtle, as for land, with an amplitude ($A_{MJO,sk}(\phi_{DC,bc})$) of 0.41 hr for the best-fitting skew-permitting waveform (dashed white line in Figure 7d). This waveform indicates earliest DC timing ($\phi_{MJO,sk}(\phi_{DC,bc})$) at MJO Phase 4.8, and the negative skew ($\alpha_{MJO}(\phi_{DC,bc})$ = −0.36) shows that, like over land, the timing of peak precipitation gets rapidly later following this earliest point in the MJO cycle. Spatial-mean DC timing over water varies between 5.4 hr in P4 and 6.2 hr in the range P7–1. The Indian Ocean, South China Sea, and Makassar Strait marine regions (outlined in Figure 2a) fail to demonstrate a coherent single-peak oscillation in DC timing (see the brown, orange and yellow crosses in Figure 7d, which are not overlaid with a waveform approximation), although the variability in DC timing between MJO phases is stronger in each of these regions than the variability in spatial-mean DC timing over all water (varying by at least 1.5 hr in all regions). Due to the broad region of coherence across the western Java Sea, the Java Sea marine region shows a coherent MJO cycle in DC timing, best characterized by the best-fitting skew-permitting waveform ($A_{MJO,sk}(\phi_{DC,bc})$ = 1.4 hr, $\phi_{MJO,sk}(\phi_{DC,bc})$ = 6.1, $\alpha_{MJO}(\phi_{DC,bc})$ = −0.52; red dashed line in Figure 7d). The spatial-mean DC timing rapidly progresses from 5.4 hr in P6 to 8.1 hr in P8, and a visibly earlier diurnal maximum during P5–6 compared to P7–2 is identified in the spatial-mean composite DCs over the Java Sea (Figure 3h). The pattern of MJO harmonic phase of DC timing over the Java Sea resembles the pattern over Sumatra and Borneo in featuring earliest DC timing around P5–6 across the western part of the region, however in contrast, there is not a coherent opposite MJO phase across the eastern part of the Java Sea marine region, and the western part shows the stronger MJO harmonic amplitude (Figure 7a). This west-east phase regime is also mirrored over the Makassar Strait; however, the stronger MJO harmonic amplitude over the eastern part of the Strait mirrors the regime over Sumatra and Borneo instead of that over the Java Sea.

The emerging pattern across most large land and sea bodies of the western MC region is that western parts of bodies experience a later-than-usual DC and eastern parts of bodies experience an earlier-than-usual DC, whereas the MJO is active over the Indian Ocean (P1–2), and this pattern reverses (often rapidly) as MJO activity crosses the MC into the western Pacific Ocean (P5–6). An MJO phase-by-phase view of DC timing (Figure 8) emphasizes westward propagation patterns during P1–2 (e.g., offshore from northwest and southwest Borneo and west Sulawesi, onshore from east Sumatra and east Borneo; Figure 8h) and eastward propagation patterns during P5–6 (e.g., offshore from southeast Sumatra and east Borneo, and across the widths of Sumatra and Borneo; Figure 8c). Elements of this pattern have been demonstrated previously, such as strongest and fastest offshore propagation of precipitation from southwest Sumatra into the Indian Ocean around P2–3 leading to the earliest DC in these MJO phases (Fujita et al., 2011). This reversal in propagation direction aligns with the reversal in the direction of the low-level zonal wind (anomaly and absolute) that accompanies the arrival of the MJO active envelope over the western MC (see Figure 1 of Zhou et al., 2023, for evidence of the low-level wind reversal over Borneo).

The relationship between the MJO harmonic phase of DC timing and the MJO harmonic phase of either daily mean precipitation or DC amplitude is complex. Over Borneo, the MJO harmonic phase of DC timing is far out of phase with the MJO harmonic phase of daily mean precipitation across both the western and eastern regions (Figure 5c), suggesting that the earliest DC at any given location in Borneo occurs when daily mean precipitation is weak. This approximate phase opposition is also observed across much of western Sumatra and western Java, whereas the majority of remaining areas that show a coherent phase lag show that the earliest DC occurs within two MJO phases of maximum daily mean precipitation. Eastern Sumatra and the area around and slightly offshore of the southern southwest Sumatra coast show a positive phase lag (i.e., $\phi_{MJO,fh}(\phi_{DC,bc}) < \phi_{MJO,fh}(c)$), meaning that the earliest DC timing precedes maximum daily mean precipitation. In contrast, the west Java Sea shows a slight negative phase lag and infers that maximum daily mean precipitation shortly precedes the earliest DC timing. Central-to-eastern Java and northern Sumatra show more complex small-scale variability in phase lag, but the MJO harmonic phases tend to be closer to alignment than opposition. The complex features of these phase lag relationships are reproduced well using the OMI in place of the RMM index.

The ratios of the MJO harmonic amplitudes of daily mean precipitation and DC amplitude to the MJO harmonic amplitude of DC timing (Figures 6c and 6e) can be used to identify areas where variability of DC timing is the dominant impact of the MJO cycle. The high ratio values over Java show that both daily mean precipitation and DC amplitude show greater variability across the MJO cycle than DC timing (relative to other locations); therefore, the low variability in DC timing over Java may warrant less focus than the variability in daily mean precipitation and DC amplitude. In contrast, the lowest values of these ratios identify areas where the DC timing varies substantially despite limited change in daily mean precipitation or DC amplitude. Such low ratio values are
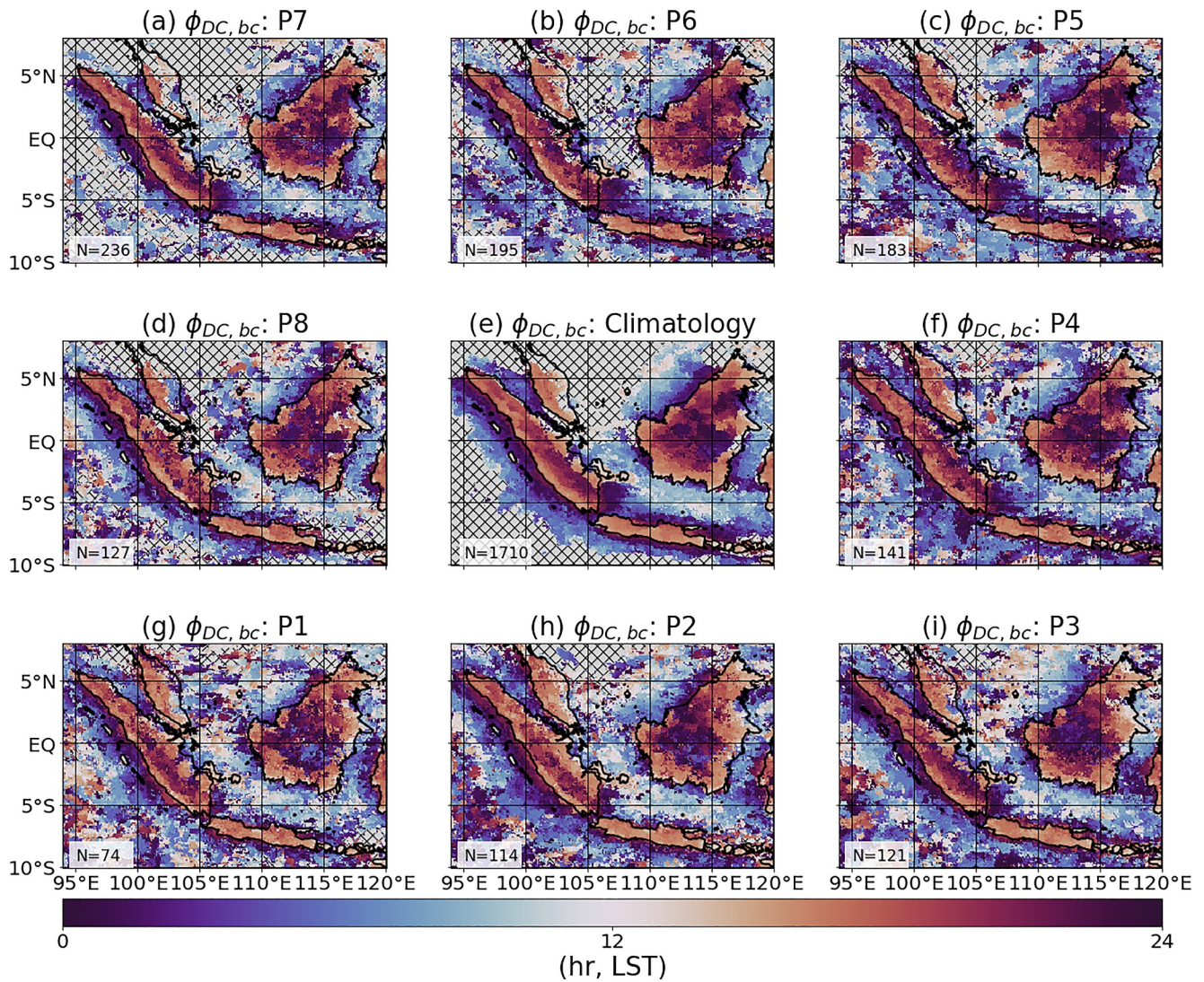
Figure 8. Explicit demonstration of the variability of DC timing through an MJO cycle. Outer panels show the time of day of the composite precipitation maximum, in LST, for each of the eight MJO phases, progressing anti-clockwise from MJO phase 1 (P1) in the bottom left panel (g). The number of days per composite is shown in the bottom left of each panel. Center panel (e) shows the climatological time of day of the composite maximum, including days with an inactive MJO. Areas with a weak diurnal cycle (half range below 0.15 mm hr^{-1}) are hatched over.

found across the Makassar Strait and the eastern parts of Sumatra and Borneo. The influence of the MJO on DC timing generally appears less strong when the DC timing is quantified using a best-fitting waveform characterization, as opposed to the peak time. For instance, the MJO harmonic amplitude of land-averaged DC timing ranges from 0.27 to 0.39 hr for the waveform-based measures of DC timing (not shown), compared to an amplitude of 0.54 hr for the MJO harmonic of peak time (solid white line in Figure 7c). Similarly, over eastern Borneo the waveform-based measures of DC timing show slightly lower MJO harmonic amplitudes in the range 1.64–1.88 hr, compared to 1.98 hr for the peak time. However, the lower influence of noise leads to a more defined regime contrast between western and eastern land areas for the MJO harmonic phase of DC timing, so the nature of the west-east phase regime divide is independent of the measure of DC timing considered.

3.4. Influence of the MJO on the Asymmetry Parameters of the Diurnal Cycle

The skew and spike asymmetry characteristics (see Section 5 of Mustafa et al., 2024) of the DC (α_{DC} and β_{DC}) each have a restricted spatial domain of relevance; these characteristics are only considered where the best-fitting

waveform provides a sufficiently accurate characterization of the (DJF climatology) composite DC, following the methodology of Mustafa et al. (2024).

Averaging across all land area with a sufficiently accurate best-fitting skew-permitting waveform characterization, there is a subtle but coherent MJO cycle in DC skew, featuring a gradual increase in spatial-mean DC skew from 0.17 in P1 to 0.26 in P8 (Figure 9c), with a rapid decrease as the MJO cycle begins again. When key land regions are considered separately, western Borneo shows the strongest and most coherent variability, ranging from spatial-mean DC skew of 0.07 in P1 to 0.26 in P6. Similarly, considering all water with a sufficiently accurate best-fitting skew-permitting waveform characterization, there is a very subtle but coherent MJO cycle in spatial-mean DC skew, ranging from 0.03 in P2 to a maximum of 0.09 in P4 (Figure 9d). The different marine regions demonstrate very distinct MJO cycles of DC skew; the Makassar Strait features especially positive DC skew in P5, whereas the Java Sea shows a gradual increase in DC skew with a rapid decrease around P6–7. Other regions, including Sumatra, eastern Borneo, the Indian Ocean and the South China Sea, do not show a coherent single-peak MJO cycle of DC skew at the regional scale. In general, the spatial distribution of DC skew values over land is most constrained in the range P4–7, with more negative and extremely positive DC skew values outside of these MJO phases (Figure 9c). The spatial distribution of DC skew values over water is, similarly, least spread in the range P2–7, though there is a great spread of DC skew values over water in all MJO phases and the contrast in spread between MJO phases is less strong than over land.

Where skew is considered relevant, maximum DC skew (Figure 9b) tends to occur around the same MJO phase as the earliest DC timing (Figure 7b). Areas including western Sumatra, western Borneo, and the western Java Sea have MJO harmonic phases of DC skew typically in the range P4–7, with the western Java Sea in particular featuring a high MJO harmonic amplitude of DC skew (Figure 9a). In contrast, the eastern Indian Ocean near southern Sumatra, the eastern Makassar Strait, and those of the eastern parts of Sumatra and Borneo that are sufficiently accurately characterized by the best-fitting skew-permitting waveform have earlier MJO harmonic phases, typically in the range P1–3. This correlation in MJO harmonic phases suggests that the timing of the diurnal minimum is less sensitive to the phase of the MJO than the timing of the diurnal maximum (the earlier the timing of the diurnal maximum, the more positive the DC skew, therefore less hours taken to intensify from the diurnal minimum). This highlights the value of considering the nature of the diurnal precipitation oscillation; a shift in the timing of the diurnal maximum does not imply that other features of the DC (such as the minimum) are equally temporally shifted.

The MJO harmonic phase of DC spike also shows spatial coherence in some regions, including central-to-eastern Borneo (P2–4), the central Java Sea (P8–2), central-to-eastern Java (P1–2), the eastern Indian Ocean around the Mentawi Islands (P7–8 around the Equator, P2 further south), and Sumatra (P6–7 along the southwest coast, P3–5 further inland to the northeast) (Figure 10b). Although not very high anywhere, the highest MJO harmonic amplitudes are found across the Java Sea and over the Indian Ocean to the south and west of the Mentawi Islands (Figure 10a), and these locations show maximum DC spike typically in the range P8–2. Although not as clear as for the MJO harmonic phase of DC timing (Figure 7b), there is some evidence of a west-east regime divide across Sumatra, Borneo, Java and the Java Sea, with western areas generally experiencing maximum DC spike around P4–7 and eastern areas generally experiencing maximum DC spike around P8–3. The divides generally appear further west than for DC timing, particularly over Borneo and the Java Sea. The regime correlation with DC timing is perhaps unsurprising; it implies that there is greater day-to-day consistency in the timing of precipitation events when precipitation occurs early via local triggering of convection than when precipitation propagates in later from elsewhere (and may propagate in at different speeds depending on the large-scale wind conditions). There is no coherent single-peak MJO cycle in spatial-mean DC spike across all land (absence of white best-fitting lines in Figure 10c); however, at the regional level, both Java and eastern Borneo show a coherent MJO cycle. The strongest coherent regional MJO cycle of DC spike over land is over eastern Borneo, where DC spike ranges from a spatial-mean minimum of 0.17 in P5 to a maximum of 0.31 in P2. This variability is discernible by eye; the spatial-mean DC across eastern Borneo shows a brief diurnal maximum in P2 and a longer-lasting maximum in P5 (Figure 3d). Over water, there is a coherent single-peak MJO cycle in spatial-mean DC spike (white dashed and dotted lines in Figure 10d), featuring a broad minimum spatial-mean DC spike of 0.11–0.13 in the range P3–7 and a maximum spatial-mean DC spike of 0.22 in P1, indicating that high DC spike before the arrival of the active MJO envelope (the eastern regime) is more dominant over water across the western MC domain. The only marine regions to demonstrate a coherent single-peak MJO cycle of DC spike are the Java Sea,
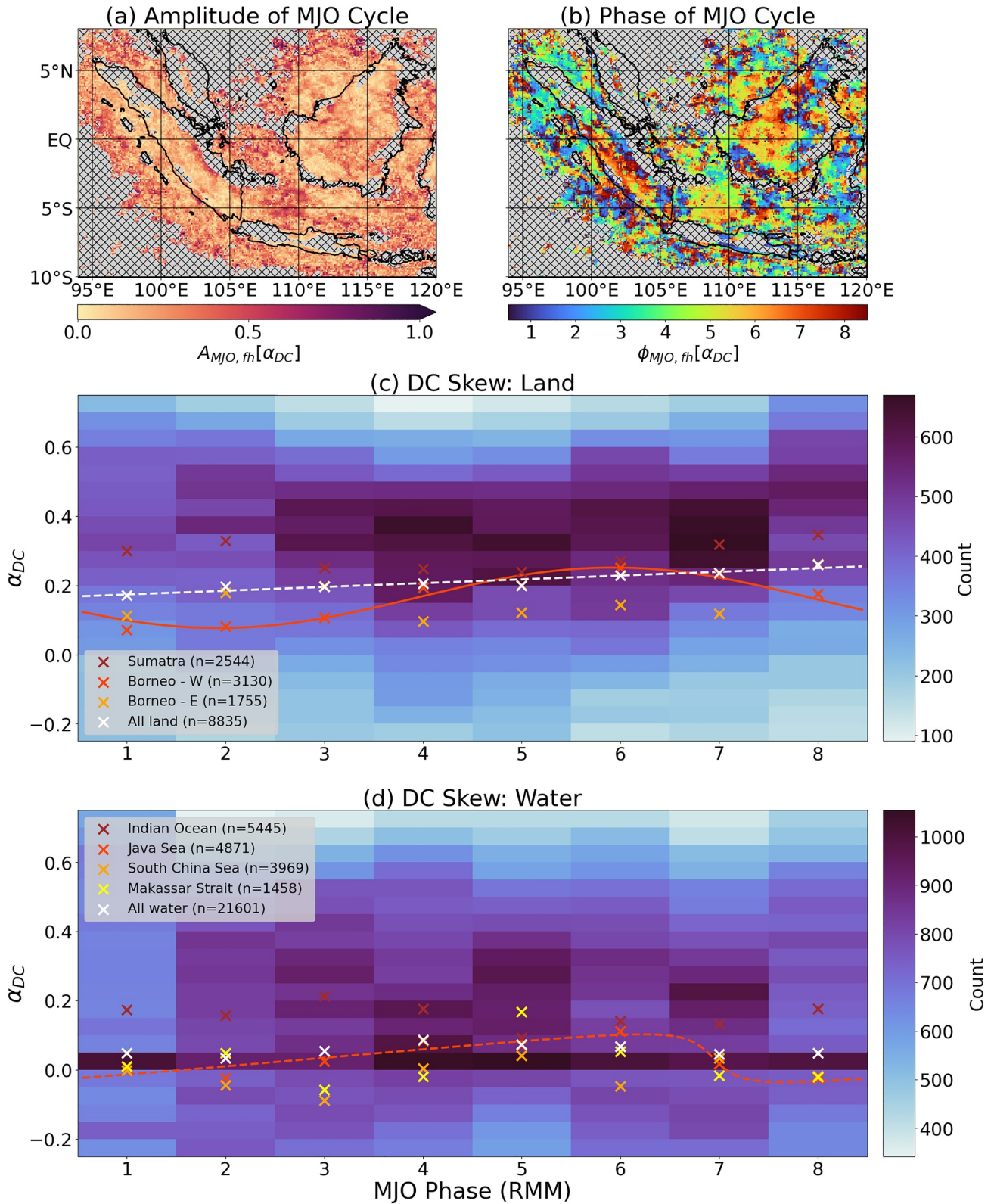
Figure 9.

where spatial-mean DC spike ranges from 0.05 in P4–5 to 0.20 in P1, and the South China Sea, where spatial-mean spike ranges from 0.10 in P5–6 to 0.23–0.24 in P8–1.

4. Discussion

This study has investigated the influence of the MJO on the DC of precipitation over the western MC as observed in the satellite-based data product IMERG v06. Comparison of the phases of the MJO harmonics of daily mean precipitation and of DC amplitude highlights a characteristic phase lag of the cycle of daily mean precipitation behind that of DC amplitude by between one quarter and one half of an MJO phase (Figure 5b), both over water and land, though with greater consistency over water. As was demonstrated by Mustafa et al. (2024), the choice of phase/timing characteristic may influence such subtle comparisons of phases/timings, and indeed the MJO phase lag is weaker based on waveform measures of DC amplitude than based on the diurnal half range, particularly over land. This discrepancy may, at least in part, be a result of the unequal distribution of days between the active MJO phases. The contribution of significantly fewer DJF days to the P1 composite likely results in a noisier DC than in surrounding MJO phases, artificially favoring higher half range and making the MJO phase of maximum DC amplitude (measured by half range) appear earlier. The waveform measures of DC amplitude, which lead to an MJO phase lag as short as 0.23 (land) and 0.40 (water) MJO phases, may therefore provide the best quantification of the lag of daily mean precipitation behind DC amplitude. The shorter lag over land appears to result from an averaging of moderate lag around near-coastal land areas and near-zero lag across inland Sumatra and central-western Borneo (Figure 5b), consistent with the findings of Sakaeda et al. (2017).

The rapid decrease in DC amplitude over land, quantified with negative skew of the MJO cycle of DC amplitude in this study, is consistent with the suggestion that the increase in cloud cover with the arrival of the MJO convective envelope rapidly damps diurnal forcing mechanisms. However, it is noted that this negative skew is not observed when compositing the MJO according to the OMI; this suggests that the influence of the dynamical component of the MJO (i.e., zonal wind anomalies) may play a key role in rapidly dampening the amplitude of the DC.

The results of the present study also consolidate the existing evidence for the phase lead of land ahead of surrounding waters, concerning both daily mean precipitation and DC amplitude (e.g., Birch et al., 2016; Oh et al., 2012; Peatman et al., 2014; Vincent & Lane, 2017). For example, Peatman et al. (2014) demonstrated a phase lead of approximately one MJO phase of both daily mean precipitation and DC amplitude over land ahead of their marine counterparts. The present study found a slightly lower phase lead, of 0.8 MJO phases for daily mean precipitation and 0.6 MJO phases for DC amplitude of the MJO harmonic of the spatial-mean land cycle ahead of the spatial-mean marine cycle. The precise values presented in this study compare land and sea broadly across the western MC region, rather than comparing specific land areas with adjacent waters. However, since there is not a strong bias in land distribution toward either the west or the east of the western MC region, it is reasoned that this broad comparison should reflect local land-sea phase contrasts reasonably well.

Variability of the timing of the DC across the MJO cycle has been a more contentious topic. The methodology applied by a handful of studies to understand MJO-associated variability of the timing of the DC relied on broad spatial averaging (Lu et al., 2019; Suzuki, 2009; Tian et al., 2006), which as shown in the present study, masks strong opposing MJO cycles in different local areas. Other studies do identify a non-trivial relationship between MJO phase and DC timing (e.g., Chen & Houze, 1997; Fujita et al., 2011; Oh et al., 2012; Rauniyar & Walsh, 2011; Sakaeda et al., 2017); however, the present study is unique in considering this relationship at a grid cell level as opposed to solely considering spatial averages. The results of this study demonstrate clear shifts in DC timing of a few hours or more in some locations; the eastern parts of Sumatra, Borneo and the Makassar Strait, along with the western side of the Java Sea, show high values of the MJO harmonic amplitude of DC timing (Figure 7a). These locations experience a strong enough DC that the variability in DC timing is not likely an artifact of noise, as it may be offshore, therefore the observed dependence of DC timing on the MJO is systematic. In P1–2, the east side of land and water masses tends to experience maximum precipitation earlier than usual,

Figure 9. As for Figure 2, but for the DC skew parameter derived from the best-fitting skew-permitting waveform. Hatching is applied in panels (a) and (b) where the best-fitting skew-permitting waveform fails to characterize the composite DC sufficiently accurately. The crosses in panels (c) and (d) show the spatial-mean DC skew values of only sufficiently accurately characterized locations. The skew parameter is not considered over Java because less than 50% of grid cells (573/1247) feature a mean DC well characterized by the best-fitting skew-permitting waveform. The vertical range from -0.25 to $+0.75$ is displayed for focus, but α_{DC} values are observed to range from -1 to $+1$.
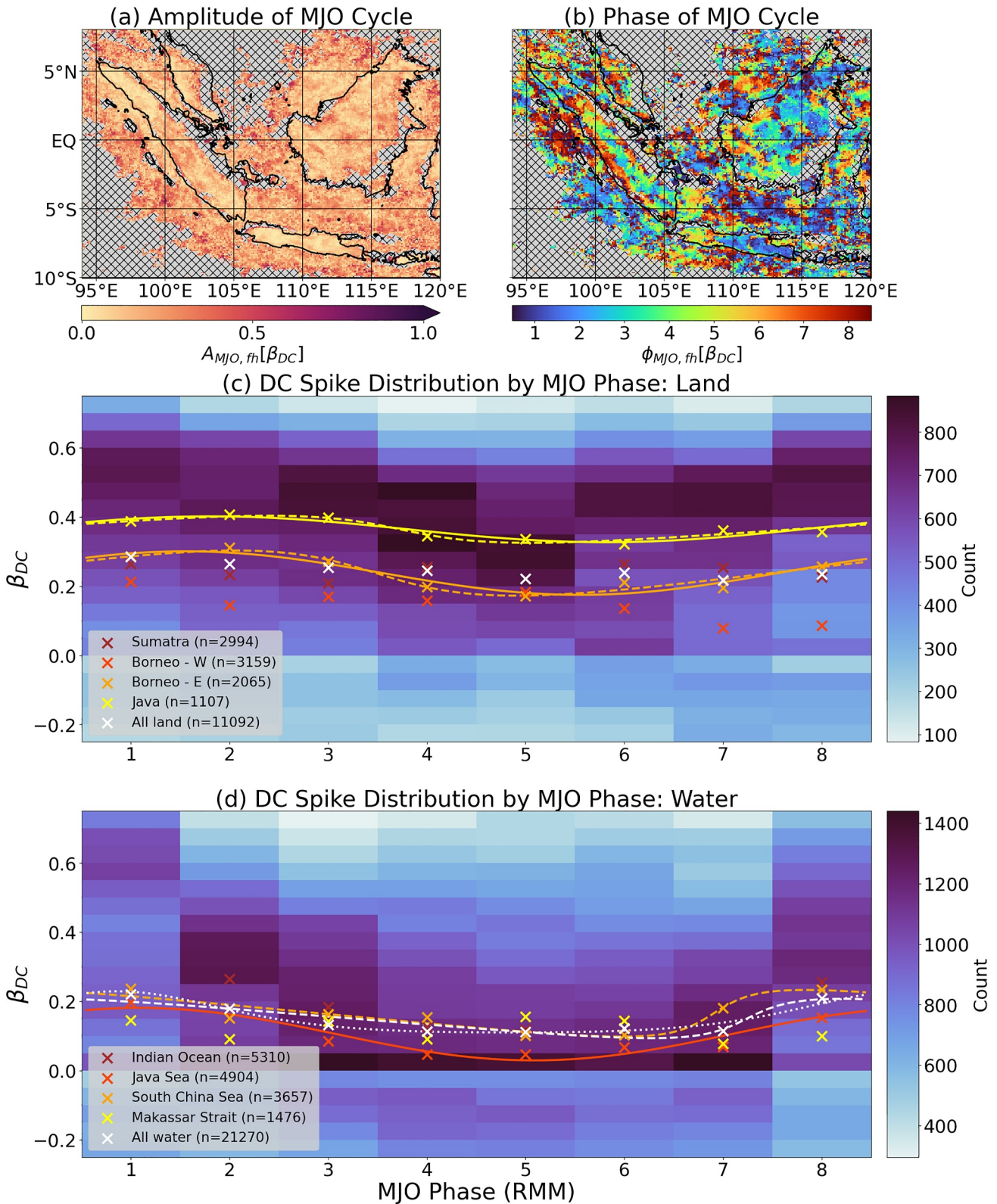
Figure 10. As for Figure 2, but for the DC spike parameter derived from the best-fitting spike-permitting waveform. Hatching is applied in panels (a) and (b) where the best-fitting spike-permitting waveform fails to characterize the composite DC sufficiently accurately. The crosses in panels (c) and (d) show the spatial-mean DC spike values of only sufficiently accurately characterized locations. The vertical range from −0.25 to +0.75 is displayed for focus, but β_{DC} values are observed to range from −1 to +1.

whereas the west side of land and water masses tends to experience maximum precipitation later than usual. By P5, when the active MJO envelope has begun to pass east of the western MC, the pattern of early and late diurnal precipitation is observed to reverse.

These changes in DC timing are symptomatic of changes to the direction of precipitation propagation, which in turn are dependent on the large-scale wind field associated with the MJO. Westward propagation of precipitation is seen during P1–2 across the Makassar Strait and inland from the east coasts of Sumatra and (less coherently) Borneo (Figures 8g and 8h). In contrast, these same locations show eastward propagation of precipitation around P5, and over Sumatra and Borneo this propagation extends across the full width of the island (Figure 8c). These propagation directions mirror the expected large-scale wind anomalies of the lower troposphere; low-level wind anomalies are directed toward the active envelope of the MJO, which is to the west of the MC over the Indian Ocean during P1–2, and to the east of the MC over the eastern MC during P5 (e.g., Lu et al., 2019).

Highly variable DC timing in certain areas (Figure 7a) typically appears to result from a change in the direction from which precipitation propagates in. Over the eastern sides of Sumatra and certain latitudinal ranges of Borneo, particularly around 2°N–4°N and 2°S–EQ, there is a strong contrast in DC timing between during P1–2 (Figures 8g and 8h), when precipitation is likely rapidly triggered in the afternoon by a sea breeze coming in from the adjacent east coast, and during P5 (Figure 8c), when maximum precipitation arrives late in the evening after propagating across the width of the island from the west coast. Meanwhile, across the stretches of western Sumatra and western Borneo close to the coastline, there is very little changeability in DC timing, with maximum precipitation seemingly invariably arriving from the adjacent western coastline in the afternoon and propagating eastward. Due to its relatively short west-east length, most locations over Sumatra fall into either the western or eastern regime described above.

The greater west-east extension of Borneo relative to Sumatra leads to more complex behavior across the center of the island. The amplitude of the MJO harmonic of DC timing is relatively low around 114–115°E north of the Equator; this region features extensive high topography, hence much convection and precipitation here is initiated by valley breeze dynamics, reducing the dependence of DC timing on the time of arrival of inland-propagating precipitation. Maximum precipitation across the high topography area typically occurs late in the evening, several hours later than near the west coast. The amplitude of the MJO harmonic of DC timing is higher to the southwest of this high topography area, with earliest DC timing around P5–6 (Figure 7b); during P5–6, eastward-propagating precipitation from the west coast of Borneo arrives relatively early in the evening, whereas during P1–2, maximum precipitation appears to propagate southwestward from the mountains through the night, often not arriving until the early hours of the morning.

Over the Makassar Strait, during P1–2 when the DC amplitude is greatest (Figure 4d), precipitation appears to be triggered by a westward-propagating land breeze triggered over Sulawesi, likely reinforced by mountain breeze dynamics. However, during P8, there is no evidence of westward propagation of precipitation across the Makassar Strait, and precipitation across the eastern Makassar Strait is triggered substantially later in the morning. Interestingly, during P5–6, the eastward propagation of precipitation across Borneo appears to continue offshore into the Makassar Strait (Figure 8c, most evident between 2°N–4°N and 2°S–EQ), which experiences notably more precipitation in the hours before sunrise in P5 than during other MJO phases (Figure 3j). This hints at the possibility of direct propagation of precipitation offshore from over Borneo without the triggering of a distinct land breeze; however, existing research suggests that convection triggered by the land breeze can be identified in close proximity to but distinct from the eastward-propagating land convection (Ichikawa & Yasunari, 2006). Over the western Java Sea, a similar phenomenon is observed as across the eastern Makassar Strait; around P5, precipitation propagates rapidly eastward from southeastern Sumatra early in the night, whereas around P1, propagation from southeastern Sumatra only extends a short distance eastward and most of the western Java Sea therefore experiences its precipitation peak much later in the morning. The variability over the Java Sea is consistent with that found by Oh et al. (2012), who also suggested that the intense precipitation in this area during the active MJO phases (specifically P5 in their study, but noted in P4 in the present study) is due to strengthened air-sea surface heat and moisture exchange resulting from the superimposing of the large-scale low-level anomalous westerlies of this MJO phase on the strong westerly mean flow over the Java Sea.

Although a robust relationship was demonstrated between the MJO cycles of daily mean precipitation and DC amplitude (Figure 5b), neither of those MJO cycles bear a consistent relationship to the MJO cycle of DC timing (Figures 5c and 5e). Some regions, such as eastern Sumatra, the western Java Sea and the eastern Makassar Strait,

show an approximate alignment of the timing of maximum DC amplitude with the timing of the earliest DC timing in the MJO cycle. Other regions, such as western Borneo, show an approximate opposition, which suggests that the timing of maximum DC amplitude is likely aligned with the latest DC timing. The alignment of the maximum in DC amplitude with a DC timing that contrasts strongly with the DC timing at other MJO phases (early or late) may diagnose areas where a mechanism for a strong DC exists only under specific large-scale conditions. In contrast, most remaining regions lack clear alignment between DC timing and DC amplitude. In such regions, there is not an approximate one-to-one relationship between DC amplitude and timing—knowing one parameter is not enough to allow reliable estimation of the other. Physical interpretation of such a lagged relationship is not straightforward and highly regionally specific, although fortunately, most of the few areas with strong systematic variability of DC timing have an approximately in-phase or opposing-phase alignment.

Changes in the timing of the DC of precipitation (Figure 8) may be related to changes in the relative proportions of convective and stratiform cloud cover. Stratiform clouds and precipitation tend to dominate within the active envelope of the MJO, whereas convective precipitation is more dominant during suppressed MJO conditions (e.g., Alber et al., 2023; Rauniyar & Walsh, 2011; Sakaeda et al., 2017). Sakaeda et al. (2017) showed that the timing of peak precipitation shows more day-to-day consistency under suppressed MJO conditions, whereas under active MJO conditions a more changeable but generally later peak time tends to be favored, proposed to be associated with the greater longevity and horizontal extent of stratiform anvils following convective events under active MJO conditions. The MJO cycle of DC spike, which generally indicates more positive spike over water during suppressed MJO phases (Figure 10d), suggests greater day-to-day consistency in the timing of diurnal activity under suppressed MJO conditions, which is consistent with the findings of Sakaeda et al. (2017). However, the regime contrast between western and eastern land masses and water masses (Figure 7b) was not noted in previous studies investigating the modulation of the DC by the MJO. Although the eastern sides of land and water masses are found in this study to experience later diurnal precipitation under and shortly after active MJO conditions, which is consistent with previous studies and the suggested mechanism of increased late stratiform precipitation, the earlier DC timing observed across the western sides of land and water masses under active MJO conditions requires explanation by an alternative mechanism. The transition from low-level easterlies to low-level westerlies during active MJO conditions may result in slightly more rapid eastward advection of convective cells away from the western sides of the large islands than during suppressed MJO conditions.

One potential impact of changes in the timing of the DC is on the balance of radiative fluxes. If the changes in the timing of the DC of precipitation found here are coupled to a DC of cloud cover of similar nature, then the proportion of daily incoming solar radiation reaching Earth's surface in different regions may be a function of MJO phase. For instance, over eastern Borneo, cloud cover in the afternoon hours around maximum precipitation at 16.4 hr during P2 (Figure 7c) would intercept more incoming solar radiation than cloud cover in the evening hours around the 20.7 hr precipitation maximum during P5. This would influence the MJO cycle of mean surface temperature in certain regions, which may influence MJO propagation. However, a more gradual intensification of precipitation in P5 may go some way to standardizing the afternoon cloud cover, and precipitation is not a sufficient indicator of cloud cover, so cloud cover data products should be consulted to investigate this possibility.

This study has investigated the modulation of the DC of precipitation by the MJO by considering variability of the various DC parameters, and has demonstrated a systematic influence of the MJO on the amplitude, phase, and asymmetric characteristics (skew and spike) of the DC. By considering the MJO cycle of the DC parameters at each grid cell, a clear west-east regime divide was identified across a range of islands and water masses, indicating westward propagation of precipitation prior to the arrival of the MJO active envelope (P1–2) and a transition to eastward propagation once the MJO active envelope has passed over to the east (P5). These results consolidate the significant modulation of the DC by the MJO that has been demonstrated in previous studies, and have shed light on the complexities of this modulation. This spatially detailed modulation benchmark across the western MC may prove a useful point of reference for future studies investigating the modulation of the DC by the MJO in weather forecasting models.

Data Availability Statement

GPM-IMERG v06 is no longer publicly available via the NASA website, since it has been superseded by v07, which is publicly available at https://disc.gsfc.nasa.gov/datasets/GPM_3IMERGHH_07/summary?keywords=%

22IMERG%20final%22. v06 is not made available alongside this study. RMM index data were sourced from http://www.bom.gov.au/climate/mjo/. OMI data were sourced from https://psl.noaa.gov/mjo/mjoindex/. The Python code used to perform waveform best-fit calculation for the skew-permitting and spike-permitting waveforms is publicly available on Zenodo (Mustafa, 2025).

References

Ahn, M.-S., Kim, D., Ham, Y.-G., & Park, S. (2020). Role of Maritime continent land convection on the mean state and MJO propagation. *Journal of Climate*, *33*(5), 1659–1675. https://doi.org/10.1175/JCLI-D-19-0342.1

Alber, K., Zhou, L., Roundy, P., & Solimine, S. (2023). Influence of the Madden-Julian Oscillation on the diurnal cycles of convection and precipitation over the Congo Basin. *Atmospheric Research*, *294*, 106967. https://doi.org/10.1016/j.atmosres.2023.106967

Bai, H., & Schumacher, C. (2022). Topographic influences on diurnally driven MJO rainfall over the Maritime continent. *J. Geophys. Res.Atmosphere*, *127*(6). https://doi.org/10.1029/2021JD035905

Birch, C., Webster, S., Peatman, S., Parker, A., Matthews, D. J., Li, Y., & Hassim, M. (2016). Scale interactions between the MJO and the western Maritime continent. *Journal of Climate*, *29*(7), 2471–2492. https://doi.org/10.1175/JCLI-D-15-0557.1

Cassou, C. (2008). Intraseasonal interaction between the Madden-Julian oscillation and the North Atlantic oscillation. *Nature*, *455*(7212), 523–527. https://doi.org/10.1038/nature07286

Chen, S., & Houze, R. (1997). Diurnal variation and lifecycle of deep convective systems over the Pacific warm pool. *Q. J. Roy. Met. Soc.*, *123*(538), 357–388. https://doi.org/10.1256/smsqj.53805

Fujita, M., Yoneyama, K., Mori, S., Nasuno, T., & Satoh, M. (2011). Diurnal convection peaks over the eastern Indian ocean off Sumatra during different MJO phases. *J. Met. Soc. Japan*, *89*, 317–330. https://doi.org/10.2151/jmsj.2011-A22

Gonzalez, A., & Jiang, X. (2017). Winter mean lower tropospheric moisture over the Maritime Continent as a climate model diagnostic metric for the propagation of the Madden-Julian oscillation. *Geophysical Research Letters*, *44*(5), 2588–2596. https://doi.org/10.1002/2016GL072430

Hagos, S., Zhang, C., Feng, Z., Burleyson, C., De Mott, C., Kerns, B., et al. (2016). The impact of the diurnal cycle on the propagation of Madden-Julian Oscillation convection across the Maritime Continent. *Journal of Advances in Modeling Earth Systems*, *8*(4), 1552–1564. https://doi.org/10.1002/2016MS000725

Hendon, H., & Salby, M. (1994). The life cycle of the Madden–Julian oscillation. *Journal of the Atmospheric Sciences*, *51*(15), 2225–2237. https://doi.org/10.1175/1520-0469(1994)051⟨2225:TLCOTM⟩2.0.CO;2

Hsu, H.-H., & Lee, M.-Y. (2005). Topographic effects on the eastward propagation and initiation of the Madden-Julian oscillation. *Journal of Climate*, *18*(6), 795–809. https://doi.org/10.1175/JCLI-3292.1

Huffman, G., Bolvin, D., Braithwaite, D., Hsu, K., Joyce, R., Xie, P., & Yoo, S.-H. (2015). NASA global precipitation measurement (GPM) integrated multi-satellitE Retrievals for GPM (IMERG). *Algorithm Theoretical Basis Document (ATBD) Version*, *4*, 26.

Ichikawa, H., & Yasunari, T. (2006). Time-space characteristics of diurnal rainfall over Borneo and surrounding oceans as observed by TRMM-PR. *Journal of Climate*, *19*(7), 1238–1260. https://doi.org/10.1175/JCLI3714.1

Kang, D., Kim, D., Ahn, M.-S., & An, S.-I. (2021). The role of the background meridional moisture gradient on the propagation of the MJO over the Maritime continent. *Journal of Climate*, *34*, 6565–6581. https://doi.org/10.1175/jcli-d-20-0085.1

Kikuchi, K., & Wang, B. (2008). Diurnal precipitation regimes in the global tropics. *Journal of Climate*, *21*(11), 2680–2696. https://doi.org/10.1175/2007JCLI2051.1

Kiladis, G., Dias, J., Straub, K., Wheeler, M., Tulich, S., Kikuchi, K., et al. (2014). A comparison of OLR and circulation-based indices for tracking the MJO. *Monthly Weather Review*, *142*(5), 1697–1715. https://doi.org/10.1175/MWR-D-13-00301.1

Kim, D., Kim, H., & Lee, M.-I. (2017). Why does the MJO detour the Maritime Continent during austral summer? *Geophysical Research Letters*, *44*(5), 2579–2587. https://doi.org/10.1002/2017GL072643

Kim, D., Kug, J., & Sobel, A. (2014). Propagating versus nonpropagating Madden-Julian oscillation events. *Journal of Climate*, *27*(1), 111–125. https://doi.org/10.1175/JCLI-D-13-00084.1

Latos, B., Lefort, T., Flatau, M., Flatau, P., Permana, D., Baranowski, D., et al. (2021). Equatorial waves triggering extreme rainfall and floods in southwest Sulawesi, Indonesia. *Monthly Weather Review*, *149*(5), 1381–1401. https://doi.org/10.1175/MWR-D-20-0262.1

Latos, B., Peyrillé, P., Lefort, T., Baranowski, D., Flatau, M., Flatau, P., et al. (2023). The role of tropical waves in the genesis of tropical cyclone Seroja in the Maritime continent. *Nature Comms*, *14*(1), 856. https://doi.org/10.1038/s41467-023-36498-w

Ling, J., Zhang, C., Joyce, R., Xie, P., & Chen, G. (2019). Possible role of the diurnal cycle in land convection in the barrier effect on the MJO by the Maritime continent. *Geophysical Research Letters*, *46*(5), 3001–3011. https://doi.org/10.1029/2019GL081962

Love, B., Matthews, A., & Lister, G. (2011). The diurnal cycle of precipitation over the Maritime Continent in a high-resolution atmospheric model. *Q. J. Roy. Met. Soc.*, *137*(657), 934–947. https://doi.org/10.1002/qj.809

Lu, J., Li, T., & Wang, L. (2019). Precipitation diurnal cycle over the Maritime Continent modulated by the MJO. *Climate Dynamics*, *53*(9–10), 6489–6501. https://doi.org/10.1007/s00382-019-04941-8

Madden, R., & Julian, P. (1971). Detection of a 40–50 Day oscillation in the zonal wind in the tropical Pacific. *Journal of the Atmospheric Sciences*, *28*(5), 702–708. https://doi.org/10.1175/1520-0469(1971)028⟨0702:DOADOI⟩2.0.CO;2

Madden, R., & Julian, P. (1972). Description of global-scale circulation cells in the tropics with a 40–50 Day period. *Journal of the Atmospheric Sciences*, *29*(6), 1109–1123. https://doi.org/10.1175/1520-0469(1972)029⟨1109:DOGSCC⟩2.0.CO;2

Mustafa, J. (2025). Single peak waveform characterisation code. (v1.0.0). https://doi.org/10.5281/zenodo.14860412

Mustafa, J., Matthews, A., Hall, R., Heywood, K., & Azaneu, M. (2024). Characterisation of the observed diurnal cycle of precipitation over the Maritime Continent. *Q. J. Roy. Met. Soc.*, *150*(762), 2602–2624. https://doi.org/10.1002/qj.4725

Neale, R., & Slingo, J. (2003). The Maritime continent and its role in the global climate: A GCM study. *Journal of Climate*, *16*(5), 834–848. https://doi.org/10.1175/1520-0442(2003)016⟨0834:TMCAIR⟩2.0.CO;2

Oh, J.-H., Kim, K., & Lim, G. (2012). Impact of MJO on the diurnal cycle of rainfall over the western Maritime Continent in the austral summer. *Climate Dynamics*, *38*(5–6), 1167–1180. https://doi.org/10.1007/s00382-011-1237-4

Peatman, S., Matthews, A., & Stevens, D. (2014). Propagation of the Madden–Julian oscillation through the Maritime continent and scale interaction with the diurnal cycle of precipitation. *Q. J. Roy. Met. Soc.*, *140*(680), 814–825. https://doi.org/10.1002/qj.2161

Peatman, S., Schwendike, J., Birch, C., Marsham, J., Matthews, A., & Yang, G.-Y. (2021). A local-to-large scale view of Maritime continent rainfall: Control by ENSO, MJO, and equatorial waves. *Journal of Climate*, *34*, 8933–8953. https://doi.org/10.1175/JCLI-D-21

Ramage, C. (1968). Role of a tropical "Maritime Continent" in the atmospheric circulation. *Monthly Weather Review*, *96*(6), 365–370. https://doi.org/10.1175/1520-0493(1968)096⟨0365:ROATMC⟩2.0.CO;2

Rauniyar, S., & Walsh, K. (2011). Scale interaction of the diurnal cycle of rainfall over the Maritime continent and Australia: Influence of the MJO. *Journal of Climate*, *24*(2), 325–348. https://doi.org/10.1175/2010JCLI3673.1

Rui, H., & Wang, B. (1990). Development characteristics and dynamic structure of tropical intraseasonal convection anomalies. *Journal of the Atmospheric Sciences*, *47*(3), 357–379. https://doi.org/10.1175/1520-0469(1990)047⟨0357:DCADSO⟩2.0.CO;2

Sakaeda, N., Kiladis, G., & Dias, J. (2017). The diurnal cycle of tropical cloudiness and rainfall associated with the Madden-Julian oscillation. *Journal of Climate*, *30*(11), 3999–4020. https://doi.org/10.1175/JCLI-D-16-0788.1

Savarin, A., & Chen, S. (2023). Land-locked convection as a Barrier to MJO propagation across the Maritime continent. *Journal of Advances in Modeling Earth Systems*, *15*(6). https://doi.org/10.1029/2022MS003503

Skinner, D., Matthews, A., & Stevens, D. (2022). North Atlantic oscillation response to the Madden–Julian oscillation in a coupled climate model. *Weather*, *77*(6), 201–205. https://doi.org/10.1002/wea.4215

Sobel, A., Maloney, E., Bellon, G., & Frierson, D. (2010). Surface fluxes and tropical intraseasonal variability: A reassessment. *Journal of Advances in Modeling Earth Systems*, *2*(1), 2. https://doi.org/10.3894/james.2010.2.2

Stachnik, J., & Chrisler, B. (2020). An index intercomparison for MJO events and termination. *Journal of Geophysical Research*, *125*(18), 125. https://doi.org/10.1029/2020JD032507

Suzuki, T. (2009). Diurnal cycle of deep convection in super clusters embedded in the Madden-Julian Oscillation. *J. Geophys. Res.Atmosphere*, *114*(D22). https://doi.org/10.1029/2008JD011303

Tan, J., Huffman, G., Bolvin, D., & Nelkin, E. (2019). Imerg V06: Changes to the morphing algorithm. *Journal of Atmospheric and Oceanic Technology*, *36*(12), 2471–2482. https://doi.org/10.1175/JTECH-D-19-0114.1

Tian, B., Waliser, D., & Fetzer, E. (2006). Modulation of the diurnal cycle of tropical deep convective clouds by the MJO. *Geophysical Research Letters*, *33*(20). https://doi.org/10.1029/2006GL027752

Vincent, C., & Lane, T. (2016). Evolution of the diurnal precipitation cycle with the passage of a Madden-Julian oscillation event through the Maritime continent. *Monthly Weather Review*, *144*(5), 1983–2005. https://doi.org/10.1175/MWR-D-15-0326.1

Vincent, C., & Lane, T. (2017). A 10-year austral summer climatology of observed and modeled intraseasonal, Mesoscale, and diurnal variations over the Maritime continent. *Journal of Climate*, *30*(10), 3807–3828. https://doi.org/10.1175/JCLI-D-16-0688.1

Wei, Y., Pu, Z., & Zhang, C. (2020). Diurnal cycle of precipitation over the Maritime continent under modulation of MJO: Perspectives from cloud-permitting scale simulations. *Journal of Geophysical Research*, *125*(13), 125. https://doi.org/10.1029/2020JD032529

Wheeler, M., & Hendon, H. (2004). An all-season real-time multivariate MJO index: Development of an index for monitoring and prediction. *Monthly Weather Review*, *132*(8), 1917–1932. https://doi.org/10.1175/1520-0493(2004)132⟨1917:AARMMI⟩2.0.CO;2

Wu, C.-H., & Hsu, H.-H. (2009). Topographic influence on the MJO in the Maritime continent. *Journal of Climate*, *22*(20), 5433–5448. https://doi.org/10.1175/2009JCLI2825.1

Yang, G.-Y., & Slingo, J. (2001). The diurnal cycle in the tropics. *Monthly Weather Review*, *129*(4), 784–801. https://doi.org/10.1175/1520-0493(2001)129⟨0784:TDCITT⟩2.0.CO;2

Zhang, C., & Ling, J. (2017). Barrier effect of the Indo-Pacific Maritime continent on the MJO: Perspectives from tracking MJO precipitation. *Journal of Climate*, *30*(9), 3439–3459. https://doi.org/10.1175/JCLI-D-16-0614.1

Zhou, Y., Wang, S., & Fang, J. (2023). Diurnal cycle and dipolar pattern of precipitation over Borneo during the MJO: Linear theory and nonlinear sensitivity experiments. *J. Geophys. Res.Atmosphere*, *128*(5). https://doi.org/10.1029/2022JD037616